Mon. Not. R. Astron. Soc. 000, 1–?? (1994) Printed 29 March 2005 (MN LaTeX style file v1.4)

Origin of E+A galaxies: I. Physical properties of E+A's formed from galaxy merging and interaction

K. Bekki,[1] W. J. Couch[1] Y. Shioya[2], and A. Vazdekis[3]
[1] *School of Physics, University of New South Wales, Sydney 2052, NSW, Australia*
[2] *Astronomical Institute, Tohoku University, Sendai, 980-8578, Japan*
[3] *Instituto de Astrofisica de Canarias, La Laguna 38200, Tenerife, Spain*

Accepted Received in original form 2001

ABSTRACT

We investigate the structural, kinematical, and spectrophotometric properties of "E+A" galaxies – those with strong Balmer absorption lines but no significant [OII] emission – using numerical simulations combined with stellar population synthesis codes. We particularly focus on the two-dimensional (2D) distributions of line-of-sight velocity, velocity dispersion, colors, line index in E+A galaxies formed via the interaction and merging of two gas-rich spirals. Our numerical simulations demonstrate that E+A elliptical galaxies formed by major galaxy merging have positive radial color gradients and negative radial Hδ gradients by virtue of their central poststarburst populations. Furthermore, we show that the projected kinematical and spectroscopic properties of the simulated E+A galaxies can be remarkably different for different major merger models. For example, the simulated E+A ellipticals with kinematically decoupled cores clearly show regions of strong Hδ absorption which are very flattened, with differences in rotation and velocity dispersion between the old and young stars. E+A ellipticals are highly likely to show more rapid rotation and a smaller central velocity dispersion in young stars than in old ones. E+A's formed from the strong tidal interaction between gas-rich spirals have disky morphologies with thick disks and are highly likely to be morphologically classified as barred S0s. We also provide specific predictions on the structural, kinematical, and spectrophotometric properties of young globular cluster systems in E+A's. Based on these results, we discuss the importance of spatially resolved, integral field unit spectroscopy on large (8-10m) ground-based telescopes in confirming the formation of kinematically distinct cores in elliptical galaxies produced via dissipative merging and determining the most probable physical mechanism(s) for E+A formation with disky and spheroidal morphologies.

Key words: galaxies: starburst – galaxies:evolution – galaxies: elliptical and lenticular, cD – galaxies: kinematics and dynamics – galaxies: interaction

1 INTRODUCTION

Since Dressler & Gunn (1983) discovered the enigmatic "E+A" galaxies – i.e., those with strong Balmer line absorption but no detectable emission – in distant clusters, their origin and the physical mechanisms responsible for their formation have long been discussed both observationally and theoretically. There have been two key issues which have driven much of this discussion: Firstly, what is responsible for triggering and then abruptly truncating the recent starburst that most likely gave rise to the E+A spectral signature (Poggianti et al. 1999)? Secondly, what is the evolutionary link between E+A galaxies and the prevalent blue 'Butcher-Oemler' (Butcher & Oemler 1978) population? Although the nature of E+A galaxies in distant clusters has been extensively studied observationally (Couch & Sharples 1987, Barger et al. 1996, Couch et al. 1998, Dressler et al. 1999, Galaz 2000, Tran et al. 2003), these two issues remain far from being resolved.

Another important avenue of investigation has been to study the incidence of E+A galaxies in environments *other* than distant clusters, mainly at lower redshifts using large galaxy redshift surveys. Zabludoff et al. (1996, hereafter Z96) investigated 21 low-redshift ($0.05 < z < 0.13$) E+A's identified in a sample of 11,113 galaxies observed as part of the Las Campanas Redshift Survey. They found that most of these E+A galaxies lay in the field rather than in clusters and therefore suggested that cluster environmental effects, such as interactions with the cluster gravitational potential or intracluster medium, are not responsible for E+A formation. More recently, Blake et al. (2004) conducted a similar investigation using the order of magnitude larger 2dF Galaxy Redshift Survey (2dFGRS), and found the large majority of the ∼50–250 $z \sim 0.1$ E+A galaxies in their sample were either isolated or in galaxy groups, with only $\sim 10\%$ being in rich clusters. At higher redshifts, Tran et al. (2004) investigated the fraction of E+A galaxies in a sample of ∼ 800 spectroscopically confirmed field galaxies in the range $0.3 \leq z \leq 1.0$ and found it to be $\sim 2.7 \pm 1.1\%$, which is significantly lower than that in galaxy clusters at comparable redshifts ($11 \pm 3\%$).

Recent high resolution imaging, photometric and spectroscopic studies of E+A galaxies undertaken with the *Hubble Space Telescope* (*HST*) and large ground–based telescopes have revealed a considerable diversity in the morphological, structural, and kinematical properties between E+A's. Norton et al. (2001) investigated the internal kinematics of the E+A galaxies in the Z96 sample and found that most of them were dynamically supported, with v/σ and σ ranging from $30\,\mathrm{km\,s^{-1}}$ to $200\,\mathrm{km\,s^{-1}}$ (here v is the rotational velocity and σ is the velocity dispersion). A very recent HST-based morphological study of 5 of the Z96 E+A's by Yang et al. (2004), revealed that they were bulge-dominated systems (with and without a small underlying disk) and had radial luminosity profiles qualitatively similar to those of normal "power-law" early-type galaxies. They also discovered possible young and very bright ($M_{\rm R} < -13$) globular cluster candidates around these E+A galaxies, with the number varying significantly from galaxy to galaxy. Tran et al. (2004) have also revealed the diversity in half-light radius, total luminosity, morphological type, and internal velocity dispersion between E+A's in their samples. However, Blake et al. (2004) have cautioned that there maybe some heterogeneity and hence diversity in E+A galaxy samples due to the way they are selected; E+A samples whose strong Balmer line absorption has been identified only the basis of the equivalent width measured for the Hδ (and sometimes the Hγ) line – as has generally been the case in distant cluster studies (Dressler et al. 1999) – will be contaminated by a population of disk-dominated, dusty star-forming galaxies, as well as containing *bona fide* E+A's which are spheroid-dominated and have no ongoing star formation.

This plethora of observational data on E+A galaxies, when taken in its entirety, raise many questions, the most significant being: (i) Can model(s) of galaxy interactions and merging (e.g., minor vs major merging) explain *self-consistently* the observed dynamical, photometric, and spectroscopic properties of E+A's?. (ii) What mechanism drives the formation of disky E+A's that dominates E+A populations in clusters of galaxies? (iii) Are there any evolutionary links between the disky E+A's in clusters and "passive spirals" with k-type spectra (Couch et al. 1998)? (iv) What is the origin of the positive and negative color gradients observed in E+A's? (v) Which can more self-consistently explain the very red colors of E+A's discovered both in the field and in clusters – dust extinction or a truncated IMF? (vi) Are there any differences between the structural and kinematical properties of the old and young stellar populations in E+A galaxies? (vii) Are the physical properties of bright young star clusters observed around E+A's consistent with any formation scenario of globular cluster formation? Although previous theoretical studies have tried to understand possible star formation histories of E+A galaxies (Barbaro & Poggianti 1997; Poggianti et al. 1999; Shioya & Bekki 2000; Shioya et al. 2002; 2004), they had difficulty in addressing the above questions due to the limitations of the one-zone spectrophotometric models that they adopted. In order to properly tackle the above questions, the dynamical and spectrophotometric properties of E+A galaxies need to be investigated *jointly* in an explicitly self-consistent manner. Therefore, numerical simulations combined with stellar population synthesis codes – which enable us to predict not only structural and kinematical properties but also photometric and spectroscopic ones – are indispensable in solving the above important problems related to the formation and evolution of E+A galaxies.

The purpose of this paper is to investigate the structural, kinematical, chemical, photometric, and spectroscopic properties of E+A galaxies in an explicitly self-consistent manner, thereby making considerable progress towards answering the above question. In particular, we investigate both *radial gradients* in the spectrophotometric properties as well as the *projected* (2D) distributions of Balmer absorption, rotational velocity and velocity dispersion in E+A galaxies formed from galaxy interactions and merging: We will discuss other possible mechanisms of E+A galaxy formation in our forthcoming papers. These spatial properties are the main focus of our study since current and planned spatially resolved spectroscopy with integral field units (IFUs) on 8-10m telescopes (e.g., GMOS on Gemini) is going to provide an unprecedented wealth of data on the two-dimensional distribution of spectroscopic properties for E+A's (Pracey et al. 2004). Furthermore observational studies based on the SAURON project with reasonably large field of views (e.g., Davies et al. 2001) now provide 2D spectra data of kinematics and stellar populations for the entire regions of galaxies. The simulated 2D distributions of the dynamical and spectroscopic properties will not only enable us to identify peculiar structural and kinematical behaviour (e.g., kinematically decoupled cores) associated with the young stars in E+A galaxies, but also help us to coverage on the most reasonable E+A formation models. Our models can also predict the age-, metallicity- and spatial-distributions of young GCs associated with E+A galaxies, and so we can discuss in more depth the bright young candidates recently observed by Yang et al. (2004).

The plan of this paper is as follows: In the next section, we briefly describe our numerical models for E+A formation via galaxy interactions and merging. We summarize the numerical methods and techniques by which we can calculate the spectrophotometric properties of E+A's from N-body numerical data. In §3, we present the numerical results on the physical properties of E+A's for different merger/interaction models. In §4, we use our results to address each of the seven questions mentioned above. We summarize our conclusions in §5.

In presenting our work here, we stress that we are focussing solely on those E+A galaxies formed as a result of galaxy-galaxy interactions and merging. This does not, however, rule out other mechanisms (e.g., abrupt truncation of star formation via halo gas stripping and ram pressure stripping) being responsible for the formation of E+A galaxies,

Table 1. Model parameters

model no.	f_b [a]	f_g [b]	m_2 [c]	orbit	comments
M1	0.5	0.1	1.0	PP	major merger
M2	0.5	0.2	1.0	PP	
M3	0.5	0.5	1.0	PP	
M4	0.0	0.1	1.0	IN	no bulge
M5	0.5	0.1	1.0	IN	fiducial
M6	0.5	0.2	1.0	IN	
M7	0.5	0.5	1.0	IN	
M8	1.0	0.1	1.0	IN	more massive bulge
M9	0.0	0.1	1.0	IN	no bulge
M10	0.5	0.1	1.0	RR	
U1	0.5	0.1	0.3	IN	unequal-mass merger
U2	0.5	0.1	0.1	IN	
T1	0.0	0.1	1.0	PP	tidal interaction
T2	0.0	0.2	1.0	PP	
T3	0.0	0.5	1.0	PP	
T4	0.0	0.5	1.0	RR	
T6	1.0	0.1	1.0	PP	
T7	0.0	0.1	0.1	PP	
I1	0.0	0.1	-	-	isolated disk
I2	0.5	0.1	-	-	
I3	1.0	0.1	-	-	

[a] mass ratio of bulge to disk
[b] gas mass fraction
[c] mass ratio of two merging spirals

and that different mechanisms can operate in different environments (see, for example, Barbaro & Poggianti 1997; Bekki et al. 2001a,b; Bekki et al. 2002).

2 THE MODEL

2.1 Mergers

Since the numerical methods and techniques we employ for modeling the chemodynamical and photometric evolution of galaxy mergers have already been described in detail elsewhere (Bekki & Shioya 1998, 1999), we give only a brief review here.

2.1.1 Progenitor disk galaxies

The progenitor disk galaxies that take part in a merger are taken to have a dark halo, a bulge, and a thin exponential disk. Their total mass and size are $M_{\rm d}$ and $R_{\rm d}$, respectively. From now on, all masses are measured in units of $M_{\rm d}$ and distances in units of $R_{\rm d}$, unless otherwise specified. Velocity and time are measured in units of $v = (GM_{\rm d}/R_{\rm d})^{1/2}$ and $t_{\rm dyn} = (R_{\rm d}^3/GM_{\rm d})^{1/2}$, respectively, where G is the gravitational constant and assumed to be 1.0 in the present study. If we adopt $M_{\rm d} = 6.0 \times 10^{10}$ $M_{\odot}$ and $R_{\rm d} = 17.5$ kpc as fiducial values, then $v = 1.21 \times 10^2$ km s^{-1} and $t_{\rm dyn} = 1.41 \times 10^8$ yr.

We adopt the density distribution of the NFW halo (Navarro, Frenk & White 1996) suggested from CDM simulations:

$$\rho(r) = \frac{\rho_0}{(r/r_s)(1+r/r_s)^2}, \qquad (1)$$

where r, ρ_0, and r_s are the spherical radius, the central density of a dark halo, and the scale length of the halo, respectively. The value of r_s (0.8) is chosen such that the rotation curve of the disk is reasonably consistent with observations. The bulge has a density profile with a shallow cusp (Hernquist 1990):

$$\rho(r) \propto r^{-1}(r + a_{\rm bulge})^{-3}, \qquad (2)$$

where $a_{\rm bulge}$ is the scale length of the bulge and fixed at 0.04. The bulge mass and its compactness can control the bar formation in the disks and thus the strength of starbursts in mergers. The dark matter to disk mass ratio is fixed at 9 whereas the bulge to disk ratio is assumed to be a free parameter and represented by $f_{\rm b}$. The radial (R) and vertical (Z) density profiles of the disk are assumed to be proportional to $\exp(-R/R_0)$ with scale length $R_0 = 0.2$ and to ${\rm sech}^2(Z/Z_0)$ with scale length $Z_0 = 0.04$ in our units, respectively. In addition to the rotational velocity attributable to the gravitational field of the disk and halo components, the initial radial and azimuthal velocity dispersions are added to the disk component in accordance with the epicyclic theory, and with a Toomre parameter value of $Q = 1.5$ (Binney & Tremaine 1987) . The vertical velocity dispersion at a given radius is set to be 0.5 times as large as the radial velocity dispersion at that point, as is consistent with the trend observed in the Milky Way (e.g., Wielen 1977).

The disk is composed both of gas and stars, with the gas mass fraction ($f_{\rm g}$) being a free parameter and the gas disk represented by a collection of discrete gas clouds that follow the observed mass-size relationship (Larson 1981). All overlapping pairs of gas clouds are made to collide with the same restitution coefficient of 0.5 (Hausman & Roberts 1984). The gas is converted into either *field stars* or *globular clusters (GCs)*. Field star formation is modeled by converting the collisional gas particles into collisionless new stellar particles according to the algorithm of star formation described below. We adopt the Schmidt law (Schmidt 1959) with exponent $\gamma = 1.5$ ($1.0 < \gamma < 2.0$, Kennicutt 1998) as the controlling parameter of the rate of star formation. The amount of gas consumed by star formation for each gas particle in each time step is given by:

$$\dot{\rho_{\rm g}} \propto {\rho_{\rm g}}^{\gamma}, \qquad (3)$$

where $\rho_{\rm g}$ is the gas density around each gas particle. The coefficients in the law are taken from the work of Bekki (1998, 1999) and the mean star formation rate in an isolated disk model for 1 Gyr evolution is ~ 1 $M_{\odot}$ for the adopted coefficient (thus consistent with observations). Globular cluster formation in the present model is discriminated from field star formation as follows. We use the cluster formation criteria derived by previous analytical works (e.g., Kumai et al. 1993), and hydrodynamical simulations with a variety of different parameters for cloud-cloud collisions on a 1-100 pc scale (Bekki et al. 2004) in order to model globular cluster formation. A gas particle is converted into a cluster if it collides with other high velocity gas (with the relative velocities ranging from 30 km s^{-1} to 100 km s^{-1}) and having an impact parameter (normalized to the cloud radius) less than 0.25. These stars formed from gas are called "new stars" (or "young stars") whereas stars initially within a disk are called "old stars". throughout this paper.

2.1.2 Chemical and spectrophotometric evolution

Chemical enrichment through star formation during galaxy merging is assumed to proceed both locally and instantaneously in the present study. We assign the metallicity of the original gas particles to the new stellar particles and increase the metallicity of the neighbouring gas particles. The total number of neighbouring gas particles is taken to be $N_{\rm gas}$, given by the following equation for chemical enrichment:

$$\Delta M_{\rm Z} = \{Z_i R_{\rm met} m_s + (1.0 - R_{\rm met})(1.0 - Z_i) m_s y_{\rm met}\}/N_{\rm gas}. \quad (4)$$

Here, $\Delta M_{\rm Z}$ represents the increase in metallicity for each gas particle, Z_i the metallicity of the new stellar particle (or that of the original gas particle), $R_{\rm met}$ the fraction of gas returned to the interstellar medium, m_s the mass of the new star, and $y_{\rm met}$ the chemical yield. The values of $R_{\rm met}$ and $y_{\rm met}$ are set to 0.3 and 0.02, respectively. It is assumed here that the spectral energy distribution (SED) of a model galaxy is the sum of the SEDs of the individual stellar particles. The SED of each stellar particle is assumed to be a simple stellar population (SSP) that is a coeval and chemically homogeneous assembly of stars. Thus the monochromatic flux of a galaxy with age T, $F_\lambda(T)$, is described as

$$F_\lambda(T) = \sum_{\rm star} F_{{\rm SSP},\lambda}(Z_i, \tau_i) \times m_s \ , \quad (5)$$

where $F_{{\rm SSP},\lambda}(Z_i, \tau_i)$ and m_s are the monochromatic flux of a SSP of age τ_i and metallicity Z_i (where the suffix i identifies each stellar particle), and the mass of each stellar particle, respectively. The age of each SSP, τ_i, is defined as $\tau_i = T - t_i$, where t_i is the time when a gas particle is converted into a stellar one. The metallicity of each SSP is exactly the same as that of the stellar particle, Z_i, and the summation ($\sum$) in equation (5) is done for all stellar particles in a model galaxy.

The adopted instantaneous recycling approximation means that the model does not consider the time delay between star formation and the onset of supernovae explosion. This means that although chemical enrichment associated with type II SNe (that form $\sim 10^7$ yr after star formation) can be modeled reasonably well, the one associated with SNeIa (that form $\sim 10^9$ yr after star formation) is not so correctly modeled owing to the large time delay between star formation and SNIa explosion. As a result of this, the present model can not correctly predict each chemical abundance (e.g., Mg and Fe) in E+A's: We have a plan to investigate chemical properties of E+A's in our forthcoming papers by using more sophisticated models including SNIa effects.

A stellar particle is assumed to be composed of stars whose age and metallicity are exactly the same as those of the stellar particle and the total mass of the stars is set to be the same as that of the stellar particle. Thus the monochromatic flux of a SSP at a given wavelength is defined as

$$F_{{\rm SSP},\lambda}(Z_i, \tau_i) = \int_{M_L}^{M_U} \phi(M) f_\lambda(M, \tau_i, Z_i) dM \ , \quad (6)$$

where M is the mass of the star, and $f_\lambda(M, \tau_i, Z_i)$ is the monochromatic flux of a star with mass M, metallicity Z_i and age τ_i. $\phi(M)$ is the initial mass function (IMF) of stars and M_U, M_L are the upper and lower mass limits of the IMF, respectively. In this paper, we use the $F_{{\rm SSP},\lambda}(Z_i, \tau_i)$ values calculated by Vazdekis et al. (1996) with an IMF slope of 1.3 (i.e., the Salpeter IMF). We also adopt their two different models with $M_L = 0.1\,{\rm M}_\odot$ and $1.0\,{\rm M}_\odot$.

In order to calculate the spectrophotometric evolution of merger remnants with poststarburst components, we need to assume that (1) the initial stellar disk and bulge in a merger progenitor spiral have the same age of $T_{\rm disk}$, and (2) the disk has a metallicity gradient consistent with observations. Considering the recent observations of the Galactic metallicity gradient (Friel 1995), we allocate metallicity to each disc star according to its initial position: At $r = R$, where $r(R)$ is the projected distance (in units of kpc) from the center of the disc, the metallicity of the star is given by:

$$[{\rm m/H}]_{\rm r=R} = [{\rm m/H}]_{\rm d,r=0} + \alpha_{\rm d} \times {\rm R}. \quad (7)$$

We adopt a plausible value of -0.091 for the slope $\alpha_{\rm d}$ from Friel (1995), in which the Galactic stellar metallicity gradient is estimated from Galactic open clusters. The central value of $[{\rm m/H}]_{\rm d,r=0}$ is chosen such that $[{\rm m/H}]_{\rm r=R}$ is 0.02 at the radius of 8.5 kpc (the solar radius for the Galactic disk). The merger models with the adopted metallicity gradients above are demonstrated to explain consistently the observed metallicity distribution function of the stellar halo in NGC 5128 (Bekki et al. 2003). We investigate the models with $T_{\rm disk}$ = 5, 7, 10 Gyr, because our results can be compared with the relatively nearby ($z \sim 0.1 - 0.3$) E+A's. We show only the results with $T_{\rm disk}$ = 7 Gyr in the present study, because the results do not strongly depend on $T_{\rm disk}$ for the above range of $T_{\rm disk}$. Several authors have suggested that starbursts produce a top-heavy IMF, because the formation of lower-mass stars is suppressed during such an event (e.g., Larson 1998). Considering this possible difference in the IMF between starburst phases and periods of normal star formation, we adopt $M_{\rm L}$ = 0.1 ${\rm M}_\odot$ for old stars and $M_{\rm L}$ = 1.0 ${\rm M}_\odot$ for new stars formed during starbursts in deriving $F_{\rm SSP}$ for each stellar component.

The main reason for our adopting a 'top-heavy' IMF for the young starburst component is as follows: Shioya et al. (2004) have demonstrated that poststarburst models with a normal IMF (with $M_{\rm L}$ = 0.1 ${\rm M}_\odot$) are unable to simultaneously explain the red colors and strong Hδ absorption that are seen for a subset of the E+A galaxies observed by Couch & Sharples (1987), Balogh et al. (1997), and Caldwell et al. (1999). We need either dust extinction (e.g., Shioya et al. 2004) or a top-heavy IMF (Balogh et al. 1997; Charlot et al. 1993) to explain these red-Hδ-strong E+A's where starbursts have ended: A top-heavy IMF is a possibility for explaining the origin of these red E+A galaxies. Therefore we have chosen a top-heavy IMF for the young stars in the present study. If the normal IMF is adopted for young stars, the poststarburst signature becomes rather weak in E+A phases. For example, EW(Hδ) in the standard model is 7.4 Å for $M_{\rm L}$ = 1.0 ${\rm M}_\odot$ and 1.1 Å for $M_{\rm L}$ = 0.1 ${\rm M}_\odot$ at the same time T.

The present model does not consider the effects of dust extinction on the SEDs of poststarburst galaxies, nor the effects of gaseous emission on the Balmer absorption lines (It should be stressed here that spectral indices are not affected by dust emission and Balmer lines might be affected by nebular emission). Since most of the gas in an interacting/merging pair should be consumed in the associated starburst and hence by the time it develops an E+A spectral signature, the omission of dust extinction effects is justified. We nonetheless discuss the possible important effects of dust in E+A spectra in §4. In order to incorporate gaseous emission into our model SEDs, we need to combine our N-body simulation code with *both* the adopted SSP code (Vazdekis et al. 1996) and with one that can provide emission lines luminosities (e.g., PEGASE by Fioc & Rocca-Volmerange 1997). To combine these three different numerical codes is a formidable task, particularly into our new chemodynamical model which already includes a variable IMF and globular cluster formation. Hence we will leave a full treatment of gaseous emission for a future paper. We therefore adopt the assumption that the dilution of the Balmer absorption features by emission from interstellar gas ionized by residual star formation in the post-starburst phase does not occur at all. Star formation is therefore assumed to be completely halted ~ 1.0 Gyr after the star formation associated with the starburst reaches its maximum rate. We therefore do not intend to discuss the origin of a small amount of possibly residual star formation observed in a few E+A galaxies (Miller & Owen 2001). AGN feedback effects from massive black holes on spectrophotometric properties of E+A's can be also important (Shioya & Bekki 2005).

2.1.3 Orbital configurations

In all of the simulations of merging pairs, the orbit of the two disks is set to be initially in the xy plane and the distance between the center of mass of the two disks is assumed to be 10 in our units (corresponding to 175 kpc). The pericenter distance and the eccentricity are set to be 1.0 (17.5 kpc) and 1.0 (i.e., parabolic), respectively, for most of the models. The spin of each galaxy in a merger is specified by two angles θ_i and ϕ_i, where suffix i is used to identify each galaxy. θ_i is the angle between the z axis and the vector of the angular momentum of a disk. ϕ_i is the azimuthal angle measured from the x axis to the projection of the angular momentum vector of a disk onto the xy plane. We specifically present the results of the following three models with different disk inclinations with respect to the orbital plane: A prograde-prograde model represented by "PP" with $\theta_1 = 0$, $\theta_2 = 30$, $\phi_1 = 0$; a retrograde-retrograde model ("RR") with $\theta_1 = 180$, $\theta_2 = 210$, $\phi_1 = 0$, and $\phi_2 = 0$; and a highly inclined model ("IN") with $\theta_1 = 60$, $\theta_2 = 60$, $\phi_1 = 90$, and $\phi_2 = 0$. The time taken for the progenitor disks to completely merge and reach dynamical equilibrium is less than 16.0 in our units (~ 2.2 Gyr) for most of our major merger models. We also present the results of unequal-mass merger models with the mass ratios of the two merging spirals (represented by m_2) equal to 0.1 and 0.3. Table 1 summarises the model parameters for the merger models, with major merger models and unequal-mass models labeled as "M" and "U", respectively.

2.2 Tidal interaction

The initial disk models and the numerical methods used for computing chemodynamical and spectrophotometric evolution are exactly the same for the tidal interaction models as they are for the merger models. In the tidal interaction models, the two disk galaxies do not merge with each other

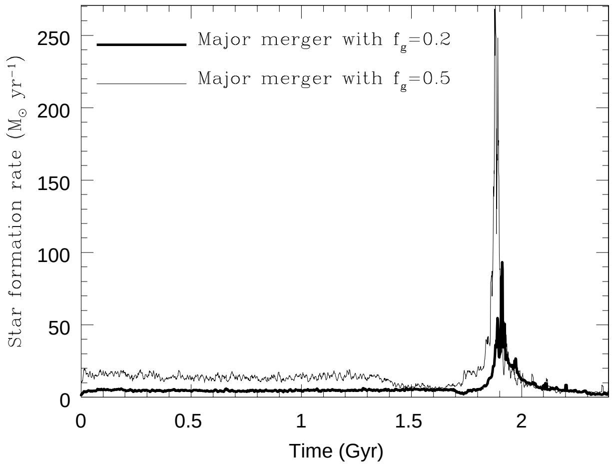

Figure 1. Star formation histories of major galaxy mergers between gas-rich spirals for the model M2 with $f_g = 0.2$ (*thin solid*) and the model M5 with $f_g = 0.5$ (*thick solid*) for 2.4 Gyr. These two models are examples of merger-driven massive starbursts with a subsequent rapid decline in star formation rate.

this possible difference of IMF between starburst phases and normal ones in galaxy evolution,

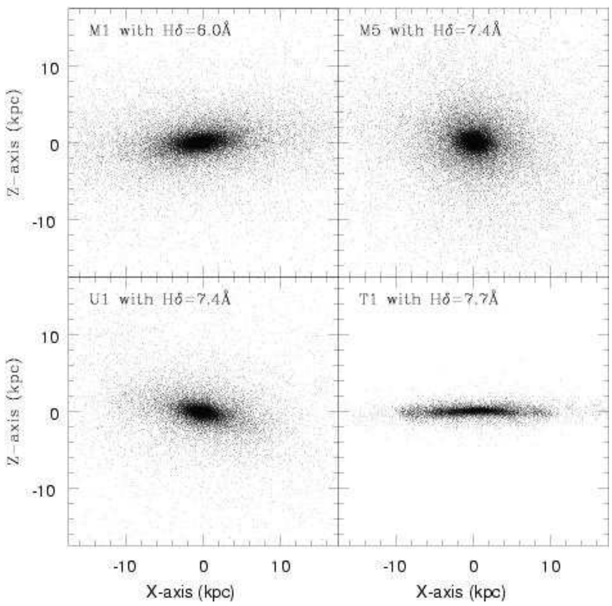

Figure 2. Mass distribution of stars of the simulated E+A's projected onto the x-z plane (corresponding to the orbital plane) for four representative models: M1 (*upper left*), M5 (fiducial, *upper right*), U1 (*lower left*), and T1 (*lower right*). EW(Hδ) in each model is shown in the upper part of each frame. Note that all models show large EW(Hδ) (≥ 6 Å).

by virtue of the large pericenter distance (2 in our units, corresponding to 35 kpc) that is adopted. Therefore, only one of the two interacting galaxies needs to be modeled as a fully self-gravitating N-body system, while the other is modeled as a point-mass particle. We mainly present the results of the tidal interaction models with $m_2 = 1.0$: Strong starbursts do not happen in interaction models with smaller m_2 (~ 0.1); hence these models do not have poststarburst populations with strong E+A spectra. Moderately strong starbursts, with a maximum star formation rate of $20-30$ $\mathrm{M}_{\odot}$, occur in tidal interactions with $m_2 = 1.0$; consequently most of the gas within interacting disks is consumed within ~ 1 Gyr.

Table 1 summarises the model parameters for the tidal interaction models, all of which are labeled "T". For comparison, we also investigated isolated disk models (without tidal interaction and merging) and these models are labeled as "I" in Table 1. The results of these isolated models are used when we investigate how strongly star formation rates are increased in interacting/merging galaxies compared with an isolated disk with no external perturbation. Star formation rates in these isolated disk models are at most a few $\mathrm{M}_{\odot}$ yr^{-1} whereas those in interacting/merging models are an order of $10-100$ $\mathrm{M}_{\odot}$ yr^{-1}. The results of the isolated models are only very briefly described in the present study, simply because they do not show E+A spectra.

All the calculations related to the above chemodynamical evolution have been carried out on the GRAPE board (Sugimoto et al. 1990) at the Astronomical Data Analysis Center (ADAC) at the National Astronomical Observatory of Japan. The gravitational softening parameter was fixed at 0.025 in our units (0.44 kpc). The time integration of the equation of motion was performed by using the 2nd-order leap-frog method. The initial total particle number in each simulation was 110,000 for a 'merger' model and 55,000 for the 'interaction' and 'isolated' models.

2.3 Main points of analysis

Star formation histories and morphological evolution of interacting and merging galaxies with strong starbursts have already been described in previous numerical studies (e.g., Noguchi & Ishibashi 1988; Mihos & Hernquist 1996; Bekki 1998). Furthermore, spectral type evolution (e.g., from "e(a)" to "a+k"; Dressler et al. 1999) in starbursting galaxy mergers has been extensively discussed by Bekki et al. (2001a) based on spectro-dynamical simulations. In this paper, therefore, we particularly focus on (1) the spatial distribution of the optical and near-infrared colors and the equivalent widths of the Balmer absorption lines in E+A's, and (2) the difference in the kinematical properties of the old and young stellar components in E+A galaxies.

As far as (2) is concerned, Norton et al. (2001) found possible differences in rotational velocity and velocity dispersion between the old and young components in nearby E+A's. Our investigation of (2) therefore involves checking whether the simulated kinematics of E+A galaxies formed by galaxy interactions and merging are consistent with such observations. The kinematical properties of the young stellar populations in E+A's are derived from the properties of the strong Balmer absorption lines, which are the key observables in this context. To compare these observables with the present numerical results in a consistent way, we show the kinematics of young H(δ) strong stars that have EW(Hδ) larger than 2Å. We attempt here to completely remove the contribution from new stars that are formed in the very early phase of merging (and thus have relatively old ages) and consequently do not contribute to the strong Balmer line absorption seen in the E+A phase.

We also investigate the physical properties of the simulated GC's in E+A's, because we consider that the predicted properties of young GC's in E+A's are useful in discussing whether the adopted cloud-cloud collision model of GC formation is consistent with the observations of young blue GC candidates in E+A's (e.g., Yang et al. 2004), and whether there are evolutionary links between blue GC candidates in E+A's and the red metal-rich GC's around passive ellipticals. We concentrate in particular on the 2D dynamical and spectroscopic distributions and the GC properties of our model merger/interaction remnant galaxies *when they have an Hδ equivalent width, EW(Hδ), larger than 6Å*, consistent with stringent criterion adopted by Z96 in their E+A selection. We here stress that when the simulated model shows strong EW(Hδ), other Balmer absorption lines also show large values: The simulated models with EW(Hδ) larger than 6Å are consistent with Z96's selection criterion.

The star formation histories, which determine the final spectrophotometric properties of the remnant interacting/merging galaxies, differ quite significantly in our simulations, being dependent on the gas mass fraction ($f_{\rm g}$), the bulge-mass fraction ($f_{\rm b}$), and the mass ratio of the merging two disks (m_2). Figure 1 shows an example of this dependence. The structural and kinematical properties of the simulated E+A's are also diverse, depending mainly on m_2 and the orbital configurations. We therefore describe the results of our most representative models which show the typical and/or most interesting behavior in E+A formation and evolution. We first describe the physical properties of the simulated E+A in the fiducial merger model M5, and then discuss their parameter dependences based on the results of other representative merger models. The morphological properties seen from the orbital plane of the galaxy interaction/merger (e.g., the x-z plane) are shown in Figure 2 for the representative models, M1, M5, U1, and T1. We mainly describe the results of these representative models.

We will explain separately the results of the merger models and the tidal interaction models, in order to contrast the differences in properties between the two. In the following sections, the time T represents the time that has elapsed since the simulation starts.

3 RESULTS

3.1 The fiducial merger model

3.1.1 2D distributions of spectrophotometric properties

Figure 3 summarises the global morphological properties of the stellar populations with different EW(Hδ) for the E+A formed in the fiducial model at $T = 2.8$ Gyr. In this major merger model with a highly inclined orbital configuration and a large pericenter distance (17.5 kpc), the old stars with EW(Hδ) < 0 Å appear to have the morphology on an elliptical galaxy. Furthermore, there is no sign of any tidal features, because the tidal tail formed during the merger disappeared by the time the remnant shows strong Balmer line absorption. The major axis of the E+A is nearly coincident with the x-axis for the old stars.

The young stars that are formed during the merger (with $0 \le$EW(Hδ) < 6Å), have more compact spatial distributions than the old stars, although their major axes are nearly aligned with those of the old stars. Young stars with EW(Hδ) > 6Å have the most compact spatial distribution,

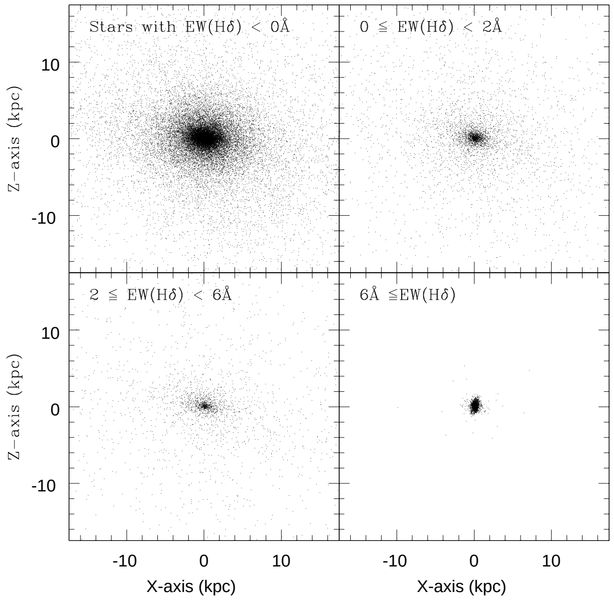

Figure 3. Mass distributions projected onto the x-z plane in the fiducial model at $T = 2.8$ Gyr for stellar populations with different EW(Hδ): For EW(Hδ) < 0 Å (upper left), $0 \leq$ EW(Hδ) < 2 Å (upper right), $2 \leq$ EW(Hδ) < 6 Å (lower left), and 6 Å $<$ EW(Hδ) (lower left).

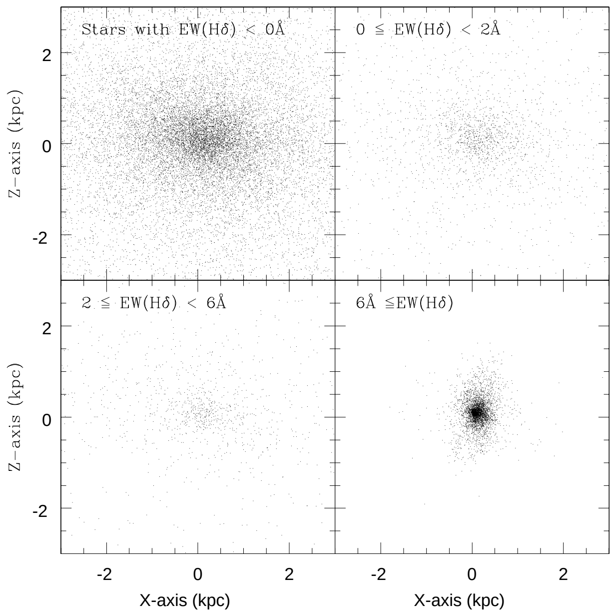

Figure 4. The same as Fig. 3 but for the central 3 kpc.

and are confined to the central few kiloparsecs. This reflects the fact that these stellar populations were formed in the last major starburst during the merger.

Figure 4 shows that there is a clear difference in the morphological properties between the old stars (with EW(Hδ) $<$ 0Å) and the youngest stars (with EW(Hδ) $>$ 6Å) within the central 3 kpc of the E+A formed in the fiducial model. In the central 3 kpc, the major axis of the old stars' mass distribution is nearly aligned with the x-axis and thus with that of the *global* mass distribution (shown

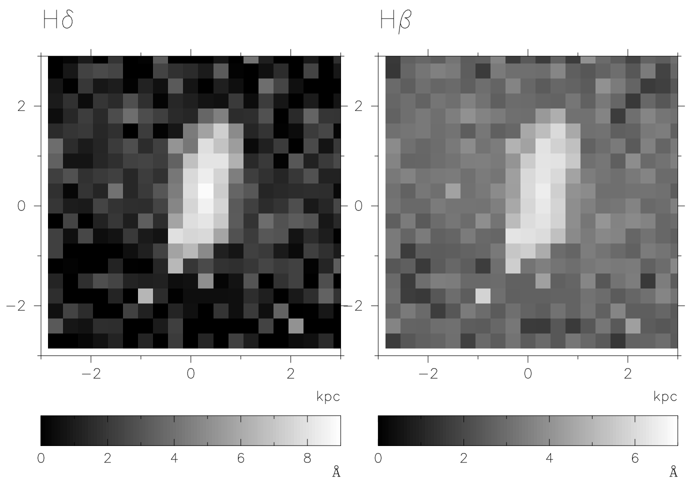

Figure 5. The two-dimensional (2D) distributions of EW(Hδ) (*left*) and EW(Hβ) (*right*) projected onto the x-z plane in the fiducial model at $T = 2.8$ Gyr. The abscissa and the ordinate represent the x-axis and the z-axis, respectively. Here we divide the 3 kpc $\times$ 3 kpc central region (shown in Fig. 4) into 20 $\times$ 20 grid points and thereby estimated the SED of each grid point. For clarity, the grid points with EW(Hδ) (and EW(Hβ)) less than 0Å are shown in the darkest color. Note that the 2D distributions show the strong Balmer line absorption to be elongated along the z-axis.

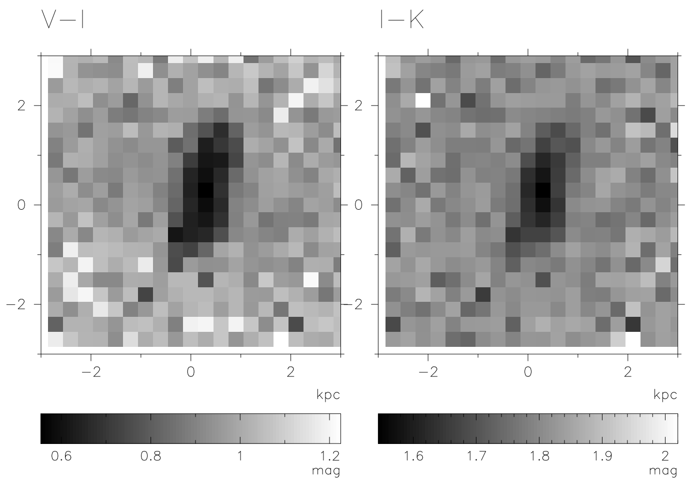

Figure 6. The same as Fig. 5 but for the optical color $V - I$ (*left*) and the near-infrared color $I - K$ (*right*).

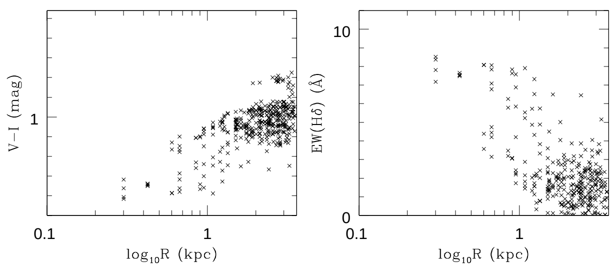

Figure 7. Radial profiles of $V - I$ (*left*) and EW(Hδ) (*right*) derived from $V - I$ and EW(Hδ) of the 400 grid points shown in Figs. 5 and 6.

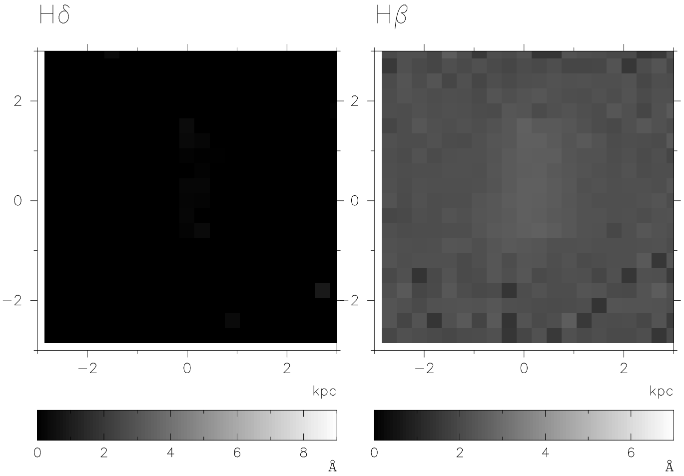

Figure 8. The same as Fig. 5 but for $T = 4.5\,$Gyr, when the model shows a passive ("k"-type) spectrum.

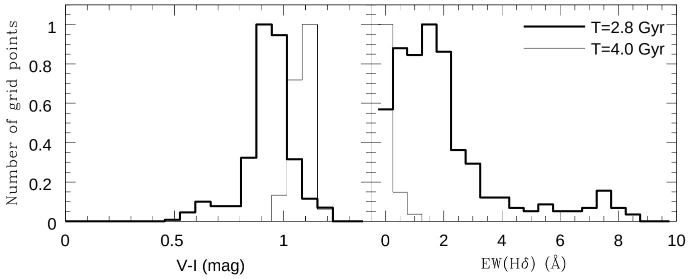

Figure 9. Distributions in the number of grid points with a given color (*left*) and EW(Hδ) (*right*) for two different epochs, $T = 2.8\,$Gyr (*thick solid line*) and $T = 4.0\,$Gyr (*thin solid line*), in the fiducial model. The color and EW(Hδ) values are those at each grid point in the 2D distributions (as shown in Figs. 5 and 6) and the normalized number of grid points is shown for convenience. The spectral type of the simulated E+A evolves from "a+k" to "k+a" (to "k") during these two epochs. Note that the dispersion of the distribution becomes very small in the k+a phase (i.e., $T = 4.0\,$Gyr) both for $V - I$ and EW(Hδ).

in Fig. 1), whereas the major axis of the young stars is nearly parallel to the z-axis (and thus perpendicular to that of the mass distribution of old stars). This misalignment in the mass distributions of the E+A results from the dissipative formation of a thick stellar disk composed of stars with strong Balmer absorption lines in the E+A core. The more diffuse distribution of young stars (with $0 \leq$EW(Hδ) < 6Å), is due to the earlier formation of these stars within the merger progenitor disks (rather than in the very center of the merger at the final phase of merging).

Figure 5 clearly shows that the 2D distributions of EW(Hδ) and EW(Hβ) absorption have very flattened shapes along the z-axis, and the direction of elongation is coincident with the major axis of the mass distribution of young stars with EW(Hδ) > 6Å(shown in Fig. 4). It also shows that both EW(Hδ) and EW(Hβ) are larger in the inner regions of the E+A, and therefore have a negative radial gradients. These results are all due principally to the centralized starbursts during dissipative merging in this model. The flattened 2D distribution can also be seen in the optical ($V-I$) and near-infrared ($I-K$) color distributions shown in Figure 6, which confirms that the flattened shape is due to the flattened distribution of young stars in the core of the E+A's.

Figure 7 shows that the radial gradient in $V - I$ color is "positive" in the sense that the inner color is bluer; this is also true for $I - K$. This figure also shows graphically, the negative radial gradients seen in EW(Hδ) and EW(Hβ). We find that the mean logarithmic gradient in $V - I$, i.e., $\Delta(V-I)/\Delta(\log R)$ is 0.14 mag per dex in radius, R, whereas that in EW(Hδ) ($\Delta H\delta/\Delta(\log R)$) is $-2.6\,$Å per dex in radius R. These positive color gradients and negative EW(Hδ) gradients in our simulated E+A's are consistent with what is observed in *some* E+A's (e.g., Yang et al. 2004). We discuss such comparisons further in §4.

In the E+A simulated in the fiducial model, the spectrophotometric properties – as delineated by the 2D distributions – rapidly evolve with time, due to the fading of the young stars. Figure 8 shows that the elongated distribution in Balmer line absorption seen in the strong E+A phase ($T = 2.8\,$Gyr) becomes nearly invisible at $T = 4.5$ Gyr (i.e., 1.7 Gyr after the strong E+A phase). This disappearance of the flattened shapes is also seen in the 2D $V - I$ and $I - K$ distributions. Figure 9 describes how the 2D $V - I$ and EW(Hδ) distributions evolve from the E+A phase to the passive ("k" type) phase. It is clear from this figure that the dispersion in the distribution becomes significantly smaller as the E+A elliptical evolves into a passive system both for $V - I$ and EW(Hδ). The $V - I$ (EW(Hδ)) dispersion decreases from 0.12 mag (2.2 Å) to 0.04 mag (0.8 Å) during the transition phase. These results suggest that the dispersion in the 2D spectrophotometric properties can be regarded as an evolutionary "time arrow" in going from the E+A phase to passive phase. We thus suggest that elliptical galaxies with

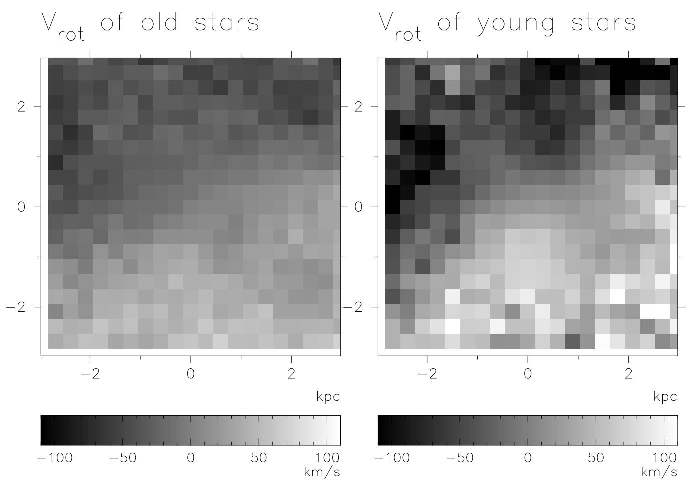

Figure 10. The 2D distribution of line-of-sight velocities viewed from the y-axis (i.e., line-of-sight velocity field projected onto the x-z plane) for old stars (*left*) and young stars (*right*) in the fiducial model at $T = 2.8\,$Gyr. The abscissa and the ordinate represent the x-axis and the z-axis, respectively. This figure enables us to confirm whether the simulated E+A has global rotation and which direction the ZVC extends. The ZVC extends from the lower left corner to the upper right corner in this figure for old stars. Each frame measures 6 kpc so that this figure can be compared with Figs. 4, 5, and 6.

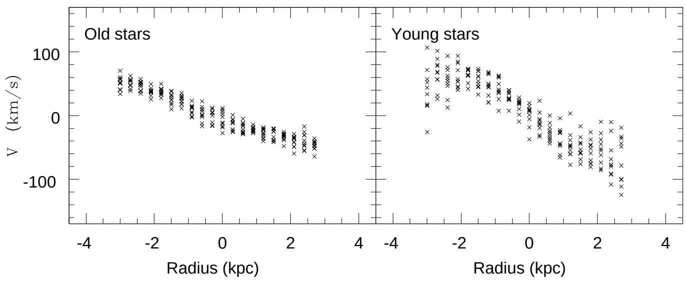

Figure 11. Radial profiles of line-of-sight velocity along the z-axis derived from grid points shown in Fig. 10 for old stars (*left*) and young stars (*right*). Note that the radial gradient is steeper for the young populations than for the old ones, though the dispersion in the outer part is large for the young ones.

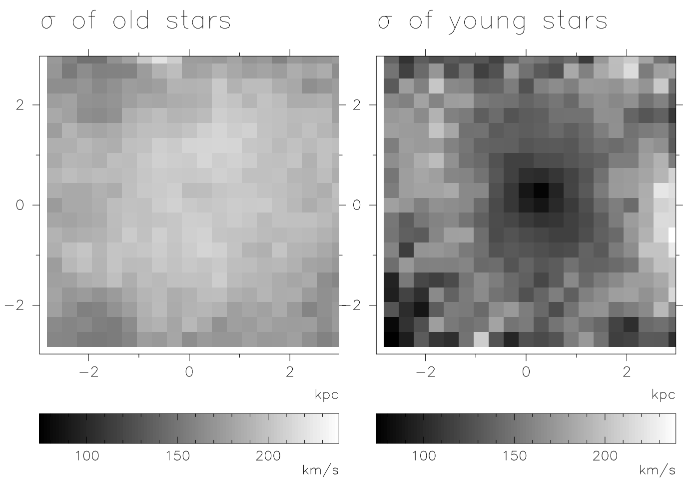

Figure 12. The same as Fig. 10 but for the velocity dispersion. Note that the young stars show smaller dispersion in the inner regions of the E+A.

weaker Hδ have smaller dispersion in the 2D distributions of colors and Balmer absorption lines.

3.1.2 Kinematics

Figure 10 displays the 2D distribution of line-of-sight-velocities for the old and young stars for the simulated E+A of the fiducial model at $T = 2.8$ Gyr. It can bee seen that for the old stars, the zero velocity curve (ZVC) – which is defined as a line connecting the points where the line-of-sight velocity is zero – extends from the lower left corner to the upper right corner and thus is not aligned with the major axis of the mass distribution of old stars shown in Figs. 3 and 4. The direction of the ZVC of young stars with EW(Hδ) ≥ 2 Å, is broadly consistent with that of the ZVC of old stars, though there is a clear difference in the velocity field along the z-axis (i.e., the vertical axis) between the two components for $|x| \leq 2$ kpc. The misalignment seen between the ZVC and the major axis of the mass distribution in E+A's, both for old and young stars, clearly indicates the minor-axis of rotation of the E+A.

Figure 11 shows the radial rotation profile along the minor axis (i.e., z-axis) derived from the data points shown in Figure 10. Figure 10 shows that the rotation profile along the minor axis is significantly different between the old stars and the young stars. By applying a least-squares fit method to the grid points with $|x| \leq 1.5$ kpc in Figure 10, we can quantify the difference in the minor-axis rotation between the two. The derived rotational velocity, $V_{\rm rot}$, expressed as a function of the z coordinate (in units of kpc), is given by:

$$V_{\rm rot} \approx -18.5 \times z - 2.5 \tag{8}$$

for the old stars, and

$$V_{\rm rot} \approx -27.0 \times z - 1.2, \tag{9}$$

for the young stars, where the velocities are in units of km s^{-1}. In the same way, the major axis rotation profile (along the x-axis) can be estimated. The derived $V_{\rm rot}$, expressed as a function of the x coordinate is:

$$V_{\rm rot} \approx 4.4 \times x - 1.9 \tag{10}$$

for the old stars, and

$$V_{\rm rot} \approx 9.3 \times x - 0.2 \tag{11}$$

for the young stars.

These results clearly indicate that the young stars are more strongly supported by rotation than the old stars in the model E+A. The origin of the steeper radial gradient of $V_{\rm rot}$ along the minor axis is closely associated with the formation of the kinematically distinct core (KDC) composed mostly of young stars with strong Hδ absorption in the central few kpc of the E+A. Owing to the efficient gaseous dissipation during the very late phase of galaxy merging, the central core can have a significant amount of rotation with the angular momentum axis different from that of the major old component. As a result of this formation of a KDC, the minor axis rotation can be more remarkable in young stars than in old ones in the 2D velocity distribution. Thus Figures 5 and 10 suggest that *future observations can confirm the dissipative formation of KDCs in galaxy mergers by investigating the 2D distribution of line-of-sight velocities of young stellar populations in E+A's.*

Figure 12 shows the 2D distribution of line-of-sight velocity dispersion (σ) both for old and young stars in the simulated E+A. Although the dispersion field appears to be somewhat irregular, in particular, for the young stars, it shows that the central dispersion is higher for the old stars than the young stars and the radial gradient of the dispersion is "positive" for young stars in the sense that the inner velocity dispersion is lower in the inner regions than in the outer regions for the central few kpc of the E+A. These two results do not depend on parameters of the present merger models, so that they can be considered to be generic characteristics of the simulated E+A's.

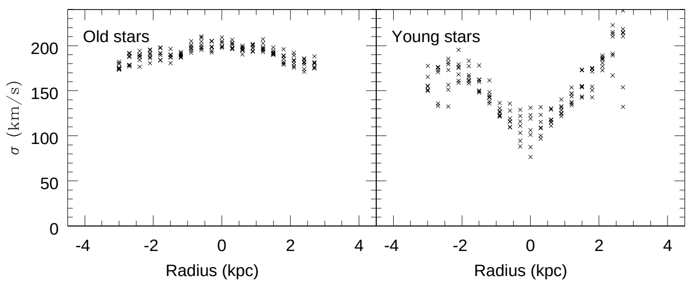

Figure 13. The same as Fig. 11 but for the velocity dispersion.

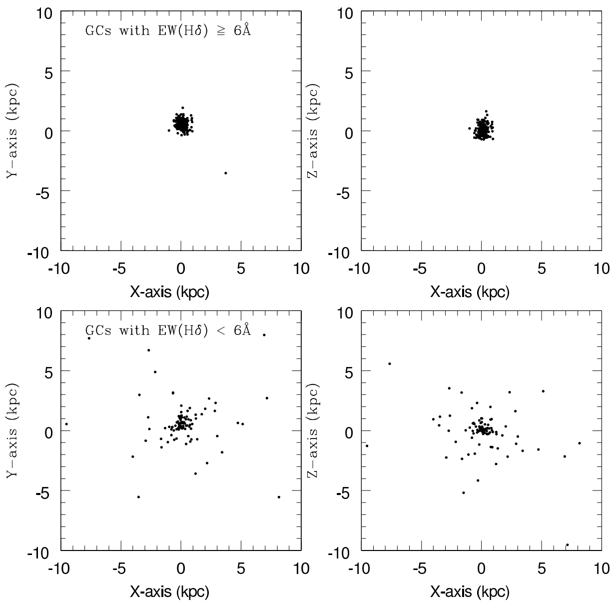

Figure 14. The distributions of young GC's with EW(Hδ) ≥ 6 Å (*upper two panels*), and with EW(Hδ) < 6 Å (*lower two panels*), projected onto the *x-y* plane (*left two panels*) and onto the *x-z* plane (*right two panels*) in the fiducial model with $T = 2.8$ Gyr.

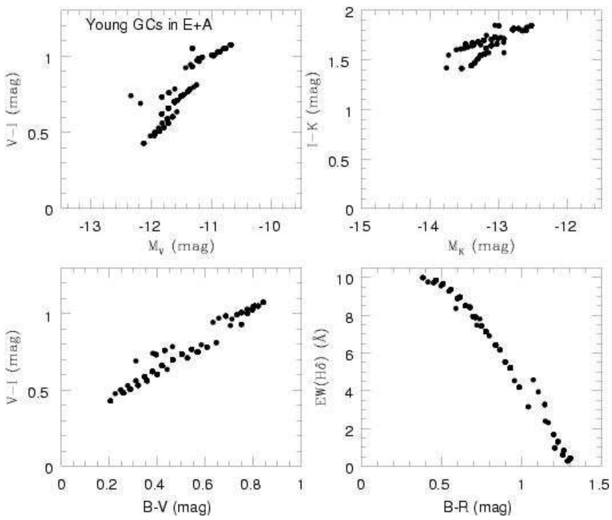

Figure 15. The distributions of young GC's on the $(V-I)$-$M_{\rm V}$ plane (*upper left*), the $(I-K)$-$M_{\rm K}$ plane (*upper right*), the $(B-V)$-$(V-I)$ plane (*lower left*), and the $(B-R)$-EW(Hδ) plane (*lower right*), for the fiducial model with $T = 2.8$ Gyr.

Figure 13 shows that the radial gradient of velocity dispersion is steeper for the young stars the older ones. If we assume $\sigma \propto R$, where R is the distance of each grid point in Figure 12 from the center of the E+A, then we can roughly quantify the difference in the radial gradient between the two components based on the least-squares fit method. The variation of the derived velocity dispersion, σ, with radius, R, for $R \leq 3$ kpc is described by:

$$\sigma \approx -11.5 \times R + 210.0 \tag{12}$$

for the old stars, and

$$\sigma \approx 8.3 \times R + 130.0 \tag{13}$$

for the young stars. The reason for the young stars apparently having such a small σ slope is that the dispersion in σ is large both at larger radii ($2-3$ kpc) and at the centrer (See Fig. 13): The least-squares fit to data points with the projected distance (R) less than 3 kpc give a small σ slope owing to this large dispersion. It should be stressed here that if the σ slope in young stars is estimated for data points with R less than 1.5 kpc, the slope becomes significantly steeper ($\sigma \propto 35 \times R$). We discuss the consistency of these results with recent observations by Norton et al. (2001) later in §4.

It should be stressed here that the positive radial gradient in velocity dispersion we see for the young stars, is consistent with the radial velocity dispersion profiles observed in bright nucleated dwarf elliptical galaxies (dE,Ns) in the Virgo cluster (Geha et al. 2002). This consistency implies that *dissipative processes associated with nuclear starbursts* can be responsible for the formation of the lower velocity dispersion nuclei in dE,N's. Given the fact that the velocity dispersion of the young stars in the E+A galaxies, EA5, EA7, and EA15, observed by Norton et al. (2001) also decreases inwardly, there could be an evolutionary link between such low luminosity E+A's and dE,Ns.

3.1.3 GC properties

Figure 14 shows the spatial distributions of young GC's formed from high-speed cloud-cloud collisions with small impact parameters in the fiducial model. The mass fraction of GC's to field stars in this model is 7%, that is a factor of ∼8 larger than that in the isolated model I1 (1%). This suggests that GC formation is more strongly enhanced than field star formation in dissipative major merging. Nearly all (100 %) of young GC's with H$\delta \geq 6$ Å are within the central 3 kpc (i.e., the projected distance of R) less than 3 kpc) of the E+A whereas about 70% of young GCs with H$\delta < 6$ Å are within the central 3 kpc, which indicates an age-dependent spatial distribution for the young GC's in the E+A (i.e., a more compact distribution for the younger GC's). This result implies that the vast majority of Hδ strong GC's will be very difficult to identify, observationally, as GC's associated with the E+A, due to their close proximity to their host's center. Only the outer young GC's with relatively small EW(Hδ) will be detected, appearing as relatively bright blue compact sources. Most of these young GC's have a metallicity that is higher than solar, and hence will evolve into red, metal-rich GC's a few Gyr later.

Figure 15 shows that young GC's in the E+A have relatively bright luminosities with $M_{\rm V} \geq$-10 mag and $M_{\rm K} \geq$ -12 mag. This is because of the young age of the GC's and the relatively high value (1.0 $M_{\odot}$) that we have adopted for the lower-mass cut off of the IMF ($m_{\rm L}$). It should be noted here that if we adopt the lower value of 0.1 $M_{\odot}$ for $m_{\rm L}$, the above absolute magnitudes of the GC's become significantly (several magnitude) fainter. Since young GCS are all assumed to have the same mass in the present study, the older (fainter) GC's will have redder colors, as shown in Figure 15. The dispersion in the optical colors, $V-I$, of the GC's is large, not because the GC's have diverse metallicities but because there are age differences between them. The GC's are actually distributed with a small dispersion along a line in the $(B-V)$-$(V-I)$ plane, due to their narrow range in metallicity.

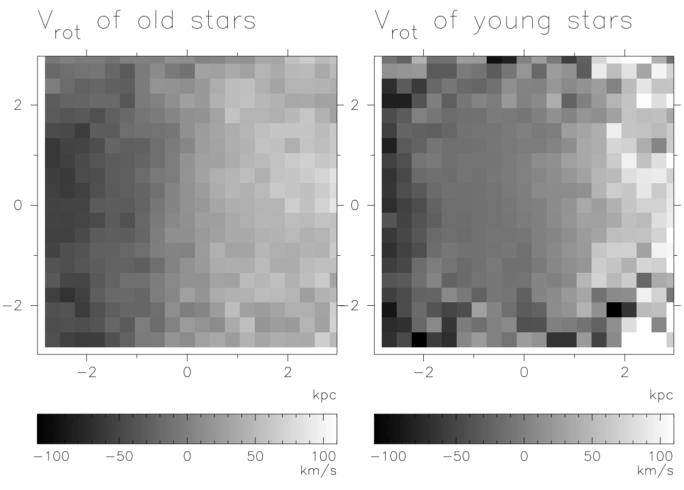

Figure 16. The same as Fig. 10 but for the model M1 at $T = 2.8\,\mathrm{Gyr}$.

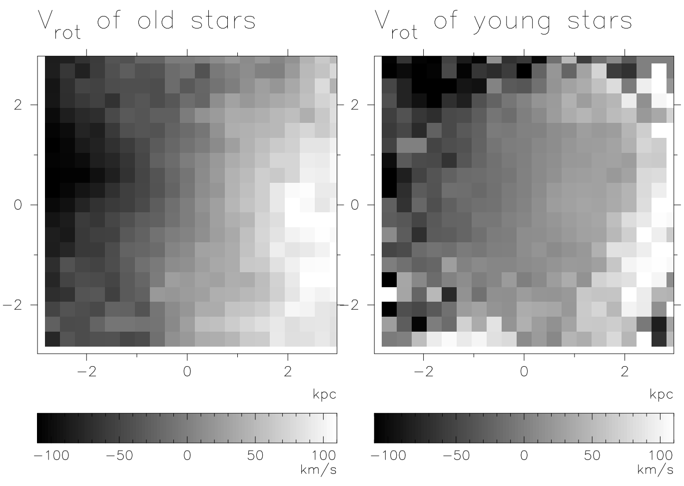

Figure 17. The same as Fig. 10 but for the model U1 at $T = 2.8\,\mathrm{Gyr}$.

The locations of the GC's on the $(B-R)$-EW(Hδ) plane in Figure 15 clearly demonstrates that they are on the "poststarburst evolutionary path" first identified by Couch & Sharples (1987), where they evolve from blue Hδ strong objects to red Hδ weak objects. Hence blue Hδ strong and red Hδ weak GC's appear to *coexist* in E+A's formed via major merging with strong starbursts. This results also implies that E+A's formed via other physical mechanisms, such as truncation of star formation without a starburst, do not show such coexistence in their GC systems. Red GC's in passive ellipticals can be either GC's that were initially associated with the merger progenitor spiral or those that were formed during dissipative merging. Bright, blue GC's with strong Hδ absorption lines in E+A's are unambiguously *young GC's formed during dissipative merging.* We therefore suggest that if the derived age-dependent spatial distribution and spectrophotometric properties of young GC's in the simulated E+A's can be compared with future observations, such theories on the formation of GC's during mergers can be tested in a more stringent way.

3.2 Parameter dependences of merger models

3.2.1 Generic results

Before discussing the dependencies our merger model results have on the various physical parameters, it is useful to summarise the more generic results of our study. These are as follows:

(i) E+A's formed by galaxy merging exhibit positive color gradients and negative EW(Hδ) gradients, due to the poststarburst populations that reside within a few kpc of their centers. By mass, the fraction of all young stars with EW(Hδ) ≥ 2 Å among all new stars can be as high as $\sim$60% in the central 3 kpc of these E+A's. The mass fraction of young stars with EW(Hδ) ≥ 2 Å among *all stars* (i.e., old + new stars) can become as high as 0.2 in the central 3 kpc. This fraction depends on the gas mass ratio of $f_{\rm g}$ in such a way that the fraction is larger for larger $f_{\rm g}$ (e.g., 0.16 for $f_{\rm g}=0.1$ and 0.20 for $f_{\rm g}=0.5$). The fractional light from these poststarburst populations in the standard model for $B-$band is ~ 60 % for $M_L = 0.1\,\mathrm{M}_{\odot}$ and ~ 100 % for $1.0\,\mathrm{M}_{\odot}$ at the strong poststarburst epoch: The SEDs of E+A's can be largely determined by young stars.

(ii) These young stars (with EW(Hδ) ≥ 2 Å) show more rapid rotation and a smaller central velocity dispersion than the old stars in the central 3 kpc of E+A's. The radial gradient in the velocity dispersion of these stars is positive in the sense that the velocity dispersion is smaller in the inner regions of an E+A.

(iii) E+A's formed in this way also have young, Hδ-strong, metal-rich (more than the solar metallicity) and blue GC's, most of which are located in their central regions. The GC formation efficiency increases dramatically (by a factor of 10) during dissipative merging, so that E+A's end up with a larger GC specific frequency (i.e., number of GCs per unit luminosity) compared to their progenitor disk galaxies. Number fraction of GC particles to all new stellar ones is $\sim$ 1 % for the isolated disk models, I1, I2 and I3 and $\sim$ 7 % for the major merger model M1.

3.2.2 Orbital configurations

Another key feature of our models is that they show the kinematical properties of the old and young stars in E+A's depend strongly on the orbital configurations of the major merger event responsible for their formation. This dependency can be summarised as follows:

(i) Some E+A ellipticals show a clear sign of major-axis rotation, yet no sign of minor-axis rotation in the 2D distribution of line-of-sight velocities for both old and young stars. Figure 16 shows an example of this for the major merger model M1 in which an E+A elliptical is formed via a nearly "prograde-prograde" merger, with the orbital spin axis nearly parallel to the intrinsic spin axes of the two merger progenitor disks. The rotational velocity, $V_{\rm rot}$ (km s^{-1}), expressed as a function of the x coordinate (kpc), that is derived for the 2D velocity distribution of the young stars in this model for $|x| \le 3$kpc is:

$$V_{\rm rot} \approx 20.1 \times x + 13.9 \qquad (14)$$

for old stars and

$$V_{\rm rot} \approx 21.7 \times x + 13.0. \qquad (15)$$

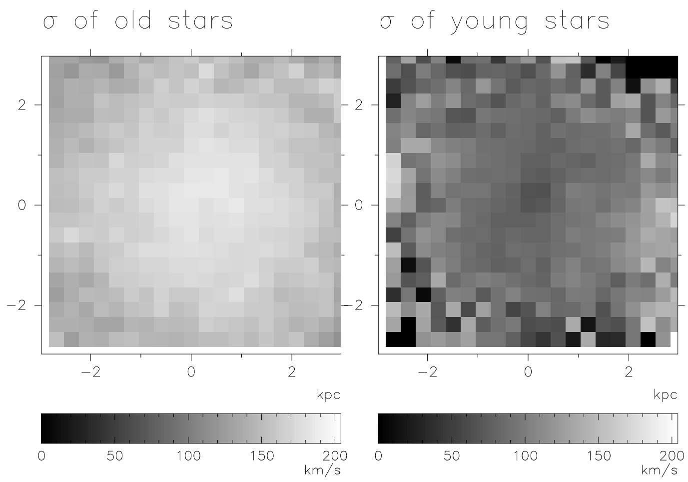

Figure 18. The same as Fig. 11 but for the model U1.

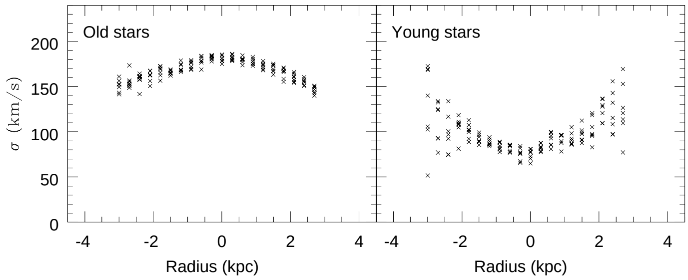

Figure 19. The same as Fig. 13 but for the model U1.

The major-axis rotation is much less remarkable for the model M10 in which an E+A is formed via a "retrograde-retrograde" merger.

(ii) Quite flattened EW(Hδ), EW(Hβ), $V-I$, and $I-K$ distributions are formed in the central few kpc of the E+A if the major merger responsible has a highly inclined orbital configuration and at least one disk orbiting in a retrograde manner (i.e., the intrinsic spin axis is anti-parallel to its orbit with respect to the mass center of the merger). The origin of the flattened distributions is due essentially to the formation of KDCs composed of young, Hδ-strong stars. Due to the presence of young KDCs, E+A ellipticals can show a significant difference in the 2D line-of-sight velocity and velocity dispersion between their old and young stars.

3.2.3 Mass ratio, m_2

The dependences of E+A properties on the merging galaxy mass ratio, m_2, can be described as follows:

(i) E+A's formed by unequal-mass mergers are highly likely to show rapid rotation along their major-axis, irrespective of the orbital configuration of the merger, if they are viewed edge-on. Figure 17 shows the 2D distributions of the line-of-sight velocities for old and young stars in the model U1, where more rapid rotation is seen than in the M1 model shown in Figure 16. This is due to the fact that the disk of the larger of the two progenitor spirals is not completely destroyed.

(ii) The positive radial gradient in the velocity dispersion of the young stars in E+A's is not as pronounced in models with smaller m_2. This is because there is less gaseous dissipation in a weaker starburst and thus the young stars with relatively cold kinematics are less centrally concentrated in these models with smaller m_2. Figures 19 and 20 show the 2D distributions of velocity dispersion and the radial profile of velocity dispersion, respectively, for old and young stars in the model U1. It is clear from these figures that even the unequal-mass model shows a difference in kinematics between the old and young stars. The variation in velocity dispersion σ (km s^{-1}) with radius, R (kpc) seen in these figures for $R \leq 3$ kpc can be described as:

$$\sigma \approx -15.1 \times R + 193.3 \quad (16)$$

for the old stars, and

$$\sigma \approx 0.2 \times R + 90.9 \quad (17)$$

for the young stars.

(iii) The mass ratio of young stars with EW(Hδ) ≥ 2 Å to all new (young) stars during the post-starburst phase, is significantly smaller for models with smaller m_2 (≤ 0.1). This is because the secondary starburst is much weaker in such models, compared to the major or unequal-mass merger models. For example, the mass ratio of the strong-Hδ young stars is only 13% in the model U2 with $m_2 = 0.1$, and 58% for the fiducial model. This suggests that minor mergers with m_2 less than 0.1 are highly unlikely to become E+A's after their secondary starbursts, due to the very small fraction of A-type stars. The present models with $m_2 = 0.1$ show EW(Hδ) of ∼2 Å and EW(Hβ) of ∼3.5 Å in their post-starburst phases. Therefore, the observed disky E+A's with strong Balmer absorption lines such as those observed in Zabludoff et al. (1996) are not likely to be formed from minor merging.

(iv) The formation efficiency of young GC's depends on m_2 in such a way that a larger number of GC's are formed during merging in the models with larger m_2. Therefore, E+A's with flattened (S0-like) morphologies formed via unequal-mass mergers show a smaller number of young GC's than those with elliptical morphologies formed via major mergers. Therefore, the observed diversity in the number of young GC candidates in E+A's (Yang et al. 2004) could be due to this diversity of m_2 in galaxy merging. Flattened E+A's are likely to show flattened spatial distributions of young GCs.

3.2.4 Miscellaneous

Finally, we note a number of other parameter dependences that our models have revealed, in particular ones involving f_g, f_b, and the IMF:

(i) It is possible that two moderately strong starbursts, separated by a time interval of ∼1 Gyr, can occur during major merging if the progenitor spirals have either no bulge (f_b =0.0) or only a very small bulge ($f_b < 0.1$). The first and stronger of these starbursts occurs as a result of the formation of a stellar bar, which in turn causes an inflow of gas into the center of the disk (e.g., in the bulgeless model M9). After this first starburst phase, the two galaxies are still separated yet at least one of them has a strong poststarburst population. The second weaker starburst then occurs when the two disks finally merge to form an elliptical. Due to the rapid consumption of gas in the first starburst, the

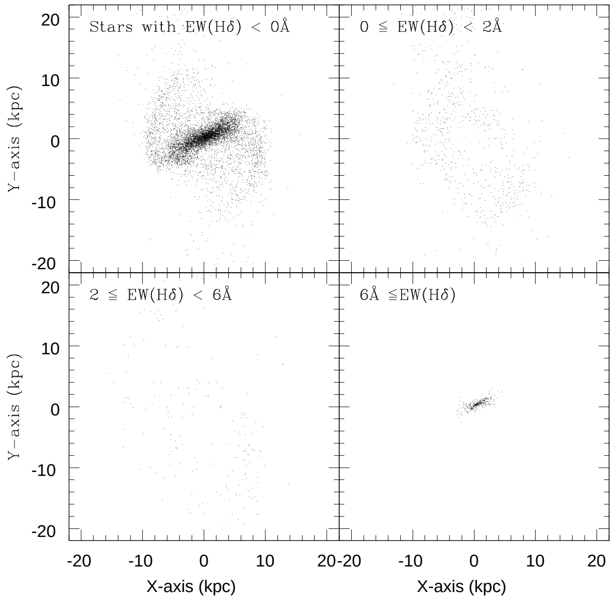

Figure 20. The same as Fig. 3 but for the model T1 projected onto the x-y plane.

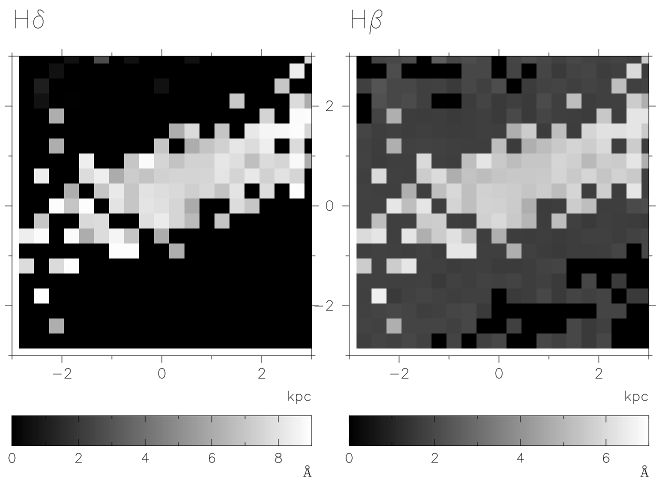

Figure 21. The same as Fig. 5 but for the model T1 projected onto the x-y plane. The abscissa and the ordinate represent the x-axis and the y-axis, respectively.

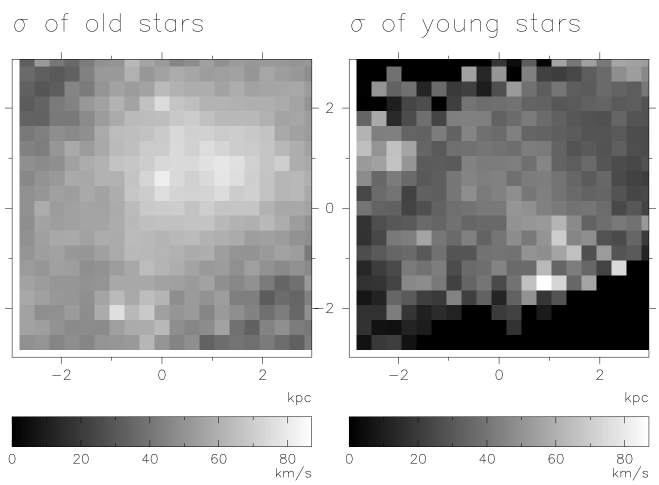

Figure 22. The same as Fig. 12 but for the model T1 projected onto the x-y plane. The abscissa and the ordinate represent the x-axis and the y-axis, respectively. The grid points with no stars are shown in the darkest color (i.e., $\sigma = 0\,\mathrm{km\,s^{-1}}$).

final E+A elliptical will, after the second starburst, have a smaller fraction of A-type stars (39% in the M9 model, compared to 58% in the fiducial model) and thus have weaker Hδ absorption (EW(Hδ) = 5.3 Å in the M9 model). In the interval between the two starbursts, such a merging system would appear as an interacting pair with an E+A spectrum, providing the star formation rate is insignificant.

(ii) The Kinematical differences between the old and young stars are larger in the models with larger $f_{\rm g}$ (i.e., larger gas mass fraction), essentially because a larger amount of random kinematical energy in the gas can be lost during merging, due to the more efficient gaseous dissipation in these models. The equivalent width of Hδ during the E+A phases does not depend strongly on $f_{\rm g}$ for a given IMF, as long as the merging galaxies are sufficiently gas-rich ($f_{\rm g} \ge 0.1$).

(iii) The equivalent width of Hδ depends strongly on the IMF of the starburst, in the sense that EW(Hδ) is larger for models with larger $m_{\rm L}$. For example, the simulated E+A in the M1 model with $f_{\rm g} = 0.1$ has EW(Hδ) = 7.4 Å for $M_{\rm L} = 1\,{\rm M}_{\odot}$ and EW(Hδ)=1.1 Å for $M_{\rm L} = 0.1\,{\rm M}_{\odot}$, whereas the E+A in the M7 model with $f_{\rm g} = 0.5$ has EW(Hδ) = 6.9 Å for $M_{\rm L} = 1\,{\rm M}_{\odot}$ and EW(Hδ) = 5.6 Å for $M_{\rm L} = 0.1\,{\rm M}_{\odot}$. In contrast, EW(Hβ) does not depend that strongly on the IMF.

3.3 Tidal interaction

In the tidal interaction model, a strong starburst will occur if the two disk galaxies are of comparable masses and they interact in a prograde manner i.e., if the intrinsic spin axis of the disk is parallel to the orbital axis. This is due to the formation of a stellar bar that drives gas into the central regions. Figure 20 shows the mass distributions of stars with different EW(Hδ) in the tidal interaction model T1, which develops a central stellar bar after the starburst. The mass distribution clearly depends on the EW(Hδ) of the stars: (i) the young stars (with EW(Hδ) ≥6 Å; *bottom right-hand panel* of Fig. 20) delineate a very compact bar in the center of the model, (ii) the old stars (with EW(Hδ) < 0Å; *top left-hand panel* of Fig. 20) delineate a global (∼10 kpc scale) bar with two spiral arms, and (iii) the intermediate age stars (with 0 ≤ EW(Hδ) < 2 Å; *top right-hand* panel in Fig. 20) appear to have a ring-like morphology.

Because of the elongated distribution of the Hδ-strong stars, the 2D distributions of EW(Hδ) and EW(Hβ) are also very flattened. Figure 21 clearly indicates that the radial gradients of EW(Hδ) and EW(Hβ) along the major axis of the flattened mass distribution of the young stars (with EW(Hδ) ≥ 6 Å) is smaller than those perpendicular to the major axis, though the radial gradients are essentially negative (i.e., large in the inner regions). The $V - I$ and $I - K$ colors also have 2D distributions with the same shapes and are also seen to have positive color gradients. Thus the simulated E+A has positive color gradients and negative gradients in EW(Hδ).

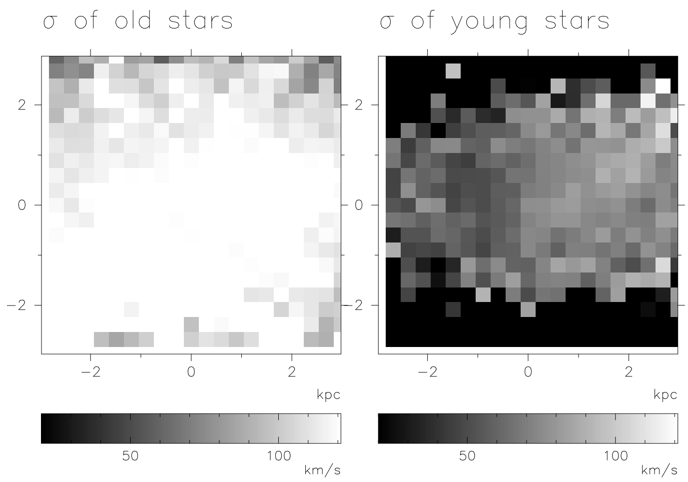

Figure 23. The same as Fig. 12 but for the tidal interaction model T1, projected onto the x-z plane. The abscissa and the ordinate represent the x-axis and the z-axis, respectively. In order to more clearly see the kinematical difference between the young and old stars, the grid points with $\sigma < 20\,\mathrm{km\,s^{-1}}$ (most of which are those where no young stars can be found) are shown in the darkest color.

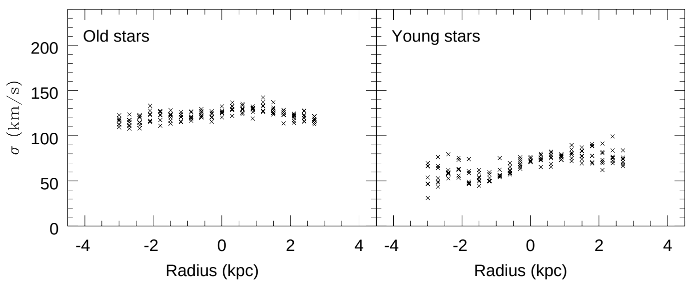

Figure 24. The same as Fig. 13 but for the tidal interaction model T1. The radial profile is derived for the 2D distribution shown in Fig. 23.

Figure 22 shows that the vertical velocity dispersion of the old stars is significantly larger than that of the young stars in the 2D distribution of velocity dispersion for the T1 model. This is because old stars are dynamically heated during tidal interaction whereas the gas, from which young stars form, dissipates its random kinematical energy during the interaction. The mean dispersion is $55.5\,\mathrm{km\,s^{-1}}$ for the old stars and $28.8\,\mathrm{km\,s^{-1}}$ for the young stars. The radial dependence of the vertical velocity dispersion, σ ($\mathrm{km\,s^{-1}}$), can be estimated from the 2D distributions shown in Figure 22 and expressed as a function of R (radius from the center of the E+A) for $R \leq 3$ kpc:

$$\sigma \approx -9.0 \times R + 76.2 \qquad (18)$$

for the old stars, and

$$\sigma \approx -11.1 \times R + 54.3 \qquad (19)$$

for the young stars. Thus the radial gradient in velocity dispersion is steeper for the young stars than the old stars.

Figures 23 and 24 reveal quite clear differences in the 2D velocity dispersion field (when viewed edge-on, i.e., in the orbital plane of the interacting galaxy) between the young and old stars. Overall, the old stars show a higher velocity dispersion than the young stars within the central 3 kpc of the simulated E+A, and a shallower radial gradient in the velocity dispersion compared with the major merger models. The young stars show a *monotonously increasing* radial profile in velocity dispersion over the range -3 kpc$\leq x \leq$ 3 kpc along the major axis (i.e., x-axis) of the mass distribution. This non-axisymmetric profile of velocity dispersion might be an indication that the young stars are in a non-equilibrium dynamical state in the E+A phase. Such a non-axisymmetric profile in velocity dispersion cannot be seen in the 2D velocity dispersion fields viewed from the x-axis and the z-axis, which implies that streaming of the gas (and young stars) along the stellar bar is partly responsible for the peculiar profile.

Formation of stellar bars is essential for triggering strong starbursts and thus for producing young poststarburst populations responsible for the E+A spectral signature. Therefore, the models in which bar formation is strongly suppressed are less likely to become E+A's. Amongst the tidal interaction models run for this study, T4 (with the disk orbiting in a retrograde manner) and T5 (with the big bulge, $f_{\mathrm{b}} = 1.0$) are less likely to become E+A's, due to the weak starbursts they experience during the tidal interaction. These results suggest that if E+A's are formed from tidal interactions between gas-rich spirals, the E+A's are more likely to be morphologically classified as barred disk galaxies, and more specifically as barred S0s due to the poor visibility of the spiral arms. Furthermore, a strong starburst associated with the formation of a stellar bar does not occur in the T6 model (where m_2 is small, being only 0.1), because the tidal perturbation is not strong enough to form a bar. Only interaction models with a large m_2 (> 0.3) show E+A spectra. This result provides a clue to the origin of the observed low luminosity disky E+A's, because lower luminosity spirals are more likely to interact with galaxies more massive than themselves. Young GC's are also formed in the interaction models, and have a 'disky' spatial distribution, quite different to that of the merger models described earlier.

4 DISCUSSION

4.1 Kinematical differences between old and young stars in E+A's

Norton et al. (2001) were the first to measure the spatially resolved kinematic properties of young and old stellar populations in E+A's and they concluded that (i) both rapidly rotating and slowly rotating or non-rotating systems can be found in the E+A phase, (ii) most E+A galaxies (70%) show no evidence for rotation, (iii) the rotation is generally seen in both the old and young stellar populations in E+A galaxies, (iv) the velocity dispersion ranges from $\sim$30 $\mathrm{km\,s^{-1}}$ to $\sim$200 $\mathrm{km\,s^{-1}}$, and (v) the young populations have *on average* a higher velocity dispersion than the old populations. In addition, Norton et al's measurements of the radial profiles in velocity dispersion for their E+A galaxy sample (see their Fig. 4), leads us to conclude that (vi) about half of the galaxies show inwardly decreasing dispersion profiles for the young stellar populations, with some at least showing the young stars to have a smaller central velocity dispersion than the old stars (e.g., EA5, EA7, and EA15).

Conclusions (i)–(iii) above are consistent with our merger models in which E+A's show a diversity in the degree of rotation of both the old and young stellar populations. The fourth conclusion can also be understood in terms of differences in the masses of the merger progenitor spirals, because more massive E+A's with a larger velocity dispersion are formed in mergers between more massive spirals with larger rotational velocities. However, conclusion (v) appears to be inconsistent with the present models in which the young stars in nearly all of the simulated E+A's show a smaller central velocity dispersion than the old stars. This inconsistency might be due to the different methods that we and Norton et al. have employed to derive the velocity dispersion of the young stars. However, it could also be due to the fact that the interstellar gas in the simulations dissipates away much more random kinematic energy during galaxy merging than actually occurs. The dynamically cold young stellar populations in the simulations could well be due to 'over-dissipation' in the gas.

Gaseous dissipation, which is responsible for the rapid gas inflow that leads to a massive starburst during merging, is essential for E+A formation as part of this process. Furthermore, the fact that our galaxy merger models are consistent with (vi) above also points to the need for efficient gaseous dissipation, since it is needed to produce dynamically cold young stellar systems. Therefore, the inconsistency between our models and conclusion (v) implies that the present numerical method for handling gaseous dissipation and star formation does not allow a proper treatment of the interstellar gas dynamics in galaxy mergers. It therefore remains unclear how the young stellar populations can have a larger velocity dispersion than the old stellar populations, if they are formed from dissipative processes of star formation.

Important factors other than the 'over-dissipation' of gas could be responsible for the larger velocity dispersion of young stars in E+A's. For example, if a massive black hole (MBH) and young A-type stars *coexist* in the central 10 pc region of an E+A, the central velocity dispersion of the young stars will be significantly higher than that of the surrounding older stars, due to the deep potential well of the MBH. If this is the case, the observed diversity in the differences in central velocity dispersion between old and young stars in E+A's could be ascribed to the existence or non-existence of MBHs in the center of E+A's. Thus two key lines of investigation in future studies will be to investigate whether an improvement in our numerical modeling of the interstellar gas leads to more consistent agreement with (v) above, and whether central MBHs in the progenitor galaxies influence the radial profiles in velocity dispersion in E+A's formed via interactions and merging.

4.2 Origin of negative color gradients in E+A's

The color gradients in E+A galaxies can be considered to be one of the key physical properties which help us to determine the most plausible physical mechanism(s) of E+A formation. This is because the spatial distribution of the most recent stars formed in an E+A depends strongly on how the star formation was truncated, and this is well traced by the color gradients (e.g., Rose et al. 2001). Bartholomev et al. (2001) investigated the color gradients in 24 E+A galaxies, as well as those in 46 other galaxies with normal spectra. They found that, on average, the E+A's had more positive color gradients than the normal galaxies. This is consistent with a merger/interaction origin for the E+A signature.

However, the origin of E+A galaxies with *negative* color gradients – which are observed both in the field and in clusters (e.g., Bartholomew et al. 2001, Yang et al. 2004) – remains unclear. In particular, the central red colors in E+A's *with negative Hδ gradients* (e.g., EA2 and EA4 in Yang et al. 2004) are not easily explained within the interaction/merger scenario for E+A formation. We suggest here three possible explanations for the existence of E+A galaxies with negative color gradients:

Firstly, the redder central colors maybe due to heavier dust extinction associated with the central poststarburst population. The question then is why do only a fraction of E+A's have dusty gas surrounding their A-type stellar populations, and how can dusty gas still exist given that most of the residual gas should be blown away from the central regions of E+A's by supernovae explosions associated with the secondary starburst?

A second possible explanation is that the IMF during the starburst is truncated, in that no stars with masses smaller than 2 $M_{\odot}$ are formed. Hence the poststarburst populations would be dominated by red evolved stars (rather than by blue, main-sequence stars), which would give rise to the redder colors in the E+A phase (Charlot et al. 1993). The problem with this scenario is that it is unclear under what physical conditions the formation of stars with masses smaller than 2 $M_{\odot}$ can be *preferentially* suppressed.

Another possible explanation is that E+A's with negative color gradients are actually not poststarburst galaxies but are starburst galaxies heavily obscured by dust. Although there is marginal evidence that some cluster galaxies with E+A spectra show radio emission that could be powered by star formation activity (Smail et al. 1999), radio continuum observations by Miller & Owen (2001) of the field E+A's in Zabludoff et al's (1996) sample yielded only 2 detections, with radio luminosities consistent with only a moderate level of star formation (inconsistent with vigorous starbursts with $10 - 100$ $M_{\odot}$). Furthermore, ultra-luminous infrared galaxies, some of which are believed to be dusty starburst galaxies, do not have E+A spectra, but rather "e(a)" spectra where [OII]λ3727 emission is seen in addition to the strong Balmer line absorption (Poggianti & Wu 2000).

Unfortunately, the data currently available for E+A galaxies does not allow us to constrain the degree of dust extinction, the exponent of the IMF, nor the spatial distribution of dust. Therefore it is not possible at the moment to determine which of the above three explanations are the most likely. It should be stressed that we have assumed in this present study that most E+A galaxies are formed from galaxy interactions and merging. It might be necessary to relax this assumption to the extent that two or more physical processes might be responsible for E+A formation. We will discuss this possibility in our forthcoming papers.

So far we did not discuss color gradients of E+As formed by merging *between an old giant elliptical and a gas-rich spiral*, because no theoretical studies (including the present one) have investigated spectrophotometric evolution of this type of galaxy mergers. Although it is not clear this 'E-Sp' merging can create E+A's, it is doubtlessly worthwhile for us to investigate this possibility in our future papers, given the fact that some Es show positive Balmer line gradients. E+A's formed by E-Sp merging could show positive color gradients, if poststarburst components originally in the spiral progenitors are dispersed into the outer parts of the remnants (owing to the tidal destruction of the spirals) and thus located in the outer part of the remnants.

4.3 Origin of kinematically decoupled cores in elliptical galaxies

About one third of nearby luminous elliptical galaxies are observed to show peculiar core kinematics, such as counter– or oddly–rotating cores, and are thus considered to have rapidly spinning thick disks or torus-like components (see Bender 1996 for a review). Numerical simulations by Hernquist & Barnes (1991) showed that ellipticals with counter-rotating cores can originate from *dissipative* major galaxy merging between two spirals. If E+A ellipticals are formed by dissipative major merging, as shown in the present study, the implication therefore is that a significant fraction of E+A's must possess kinematical distinct cores (KDCs) that are very bright and have strong Hδ absorption. Although Norton et al. (2001) have already investigated possible differences between the kinematics of the old and young stellar populations, they did not find significant kinematical differences between the two populations. However, their results are based on long-slit spectroscopy of the stellar populations in only the central few kiloparsecs of E+A galaxies, and it remains unclear whether the kinematics of this region are different to those in the more outer regions.

The present simulations have demonstrated that an E+A galaxy formed in a major merger will have a very flattened 2D distribution in Hδ, resulting from the central disky core composed mostly of A-type stars. They have also shown that the 2D kinematical distributions of the young stars are significantly different from those of the old stars, which reflects the fact that the young stellar population in the core is more strongly supported by rotation. These results suggest that E+A galaxies might well be the best 'signposts' of KDC formation in dissipative major merging. Future spatially resolved, integral field unit spectroscopy of E+A galaxies with 8-10 m class telescopes should be capable of mapping their 2D kinematical and spectral properties to the level required to address the origin of KDCs in ellipticals. If such observations also confirm the diversity in the 2D Hδ and kinematical distributions seen in our simulations, they will also confirm the dissipative major merger scenario for E+A formation.

4.4 Formation of disky E+A's

Recent morphological studies of E+A's have revealed that they are not all spheroidal systems, with a certain fraction having disks, and some of these being disk-dominated (Blake et al. 2004; Tran et al. 2004). Moreover, there seems to be environmental differences in that more 'disky' E+A galaxies are seen in rich clusters (up to $\sim$20% of the E+A population; Tran et al.) than in the lower-density group and field environment (only a $\sim$5% fraction; Blake et al.). These trends might suggest that different physical mechanisms are responsible for E+A formation in clusters and in groups/the field. Ram-pressure effects in clusters of galaxies are suggested to enhance star formation activity in gas-rich spirals without destroying their disk components (e.g., Bekki & Couch 2003, Milvang-Jensen et al. 2003; Bamford et al. 2004) and thus can be considered to contribute to the large fraction of disky E+A's in clusters. Since galaxy interactions and merging are thought to only take place in the galaxy group and field environments, the presence of disky E+A's raises the question as to what kinds of galaxy interactions and merging lead to the formation of E+A's with this morphology.

Our numerical simulations have demonstrated that: (i) rotationally supported and flattened E+A's with an S0 morphology, can be formed in *some* unequal-mass mergers, and (ii) E+A disk galaxies with thick disks can be formed in galaxy interactions with special initial parameters (e.g., prograde encounters). The latter of these is always associated with bar formation and double spiral arms (rather than multiple-arm structures). These results suggest that unequal-mass mergers are only responsible for the formation of E+A's with an S0 morphology, and that tidal interactions can be responsible for the formation of E+A's with barred morphologies or those with double-arm structures. They also suggest that field E+A's without any thick disk component can only be formed by galaxy merging and interaction. The present numerical simulations have also shown that the vertical velocity dispersion of *old stars* in disky E+A's can be rather high (up to 60 km s^{-1}) owing to the dynamically hot thick disk. Therefore high-resolution imaging of the vertical structure in disky E+A's and spectroscopic determination of the velocity dispersion of their old stars can provide valuable information on the presence of dynamically hot thick disks and thus assess the viability of the disky E+A formation scenario described in this paper.

5 CONCLUSIONS

We have investigated the dynamical and spectrophotometric properties of E+A galaxies formed via galaxy interactions and merging, using gas dynamical simulations combined with stellar population synthesis codes. Our principle results can be summarised as follows:

(1) E+A ellipticals formed by dissipative major galaxy merging show positive radial gradients in color (i.e., bluer colors at their center) and negative radial gradients in Balmer absorption line strength, due to the larger fraction of A-type stars in their inner regions. These color and line index gradients become shallower as time passes by, because of the aging of the poststarburst stellar population. These numerical models, however, cannot explain the E+A galaxies that are observed to have negative radial gradients in both color and Balmer absorption line strength.

(2) The dynamical and spectroscopic properties of E+A ellipticals formed by dissipative major galaxy merging have 2D distributions which can be remarkably different, depending on the orbital parameters of the merger. Furthermore, such differences also exist between the old and young stars in these galaxies. For example, E+A ellipticals with kinematically decoupled cores (KDC's) have a very flattened Hδ absorption distribution, with differences in rotation and ve-

locity dispersion between the old and young stars. Future spatially resolved, integral field unit spectroscopy with 8-10m class telescopes should be able to bring the past KDC formation sites in young E+A ellipticals into relief and thus provide an evidence that KDCs can be formed from dissipative major merging.

(3) The 2D distributions of colors and Balmer absorption lines in E+A ellipticals show a larger internal dispersion compared with those of 'passive' ellipticals with weak Hδ ($\sim$0Å). The internal color dispersion of ellipticals formed by major merging becomes smaller as the E+A phase passes, and therefore there will be an anti-correlation between the size of this dispersion and Hδ strength in the post-E+A phase. These results imply that the large color dispersion in the 2D photometric properties of E+A ellipticals provides further evidence for the transformation from gas-rich late-type spirals into passive ellipticals.

(4) Unequal-mass galaxy merging ($m_2 \sim 0.3$) can trigger central starbursts and thus can transform two gas-rich spirals into very flattened ellipticals or S0s with an E+A spectral signature . These E+A's are flattened by rotation, with a large V/σ (> 1), and show positive radial gradients in color and negative radial gradients in Balmer line absorption. These flattened E+A's could be the missing link between gas-rich late-type spirals and passive S0s.

(5) The mass fraction of young stars with Hδ $>$ 2 Å in a merger remnant strongly depends on the mass ratio (m_2) of the two progenitor spirals in the sense that the fraction is larger in merger remnants with larger m_2. This is essentially because secondary starbursts during merging are stronger and thus produce a larger fraction of A-type stars. Therefore, it is highly unlikely that minor mergers with $m_2 < 0.1$ are responsible for E+A formation with strong Hδ (EW$>$ 6 Å).

(6) Strong tidal interaction between galaxies can also be responsible for E+A formation, although special orbital configurations (i.e., prograde encounters, larger m_2, and smaller bulges) are required for the tidal encounters. The E+A's formed from tidal interactions are likely to have an SB0 morphology, with thick disks, positive color gradients and negative Hδ gradients. Our results thus suggest that some fraction of disky E+A's with SB0 morphology may be formed via strong tidal interactions.

(7) E+A's formed by galaxy merging and interactions can have young, bright, metal-rich, and Hδ-strong GC's, mostly in the central few kiloparsecs, because the number of cloud-cloud collisions with high relative velocities and small impact parameters are dramatically enhanced during this process. Disky E+A's are more likely to show a disky distribution of young GC's and rotational kinematics in the GC population. Furthermore, the total number of young GC's is more likely to be larger in E+A ellipticals than in disky E+A's for a given luminosity, because their formation efficiency is higher in major mergers than in minor mergers and tidal interactions.

(8) The present models of E+A formation have difficulties in explaining: (i) E+A's showing both negative radial gradients in color and EW(Hδ), and (ii) E+A's where the central velocity dispersion of the young stars is larger than for the old stars. These difficulties suggest that more sophisticated numerical methods for star formation and interstellar dynamics are required to reproduce self-consistently the diversity in the radial gradients of dynamical and spectrophotometric properties of the central poststarburst populations in E+A's.

6 ACKNOWLEDGMENT

We are grateful to the referee Alfonso Aragón-Salamanca for valuable comments, which contribute to improve the present paper. KB and WJC acknowledge the financial support of the Australian Research Council throughout the course of this work. The numerical simulations reported here were carried out on GRAPE systems kindly made available by the Astronomical Data Analysis Center (ADAC) at National Astronomical Observatory of Japan (NAOJ).

REFERENCES

Abraham, R. G., et al., 1996, ApJ, 471, 694
Balogh M. L., Morris, S. L., Yee, H. K. C., Carlberg, R. G., Ellingson, E., 1997, ApJ, 488, L75
Bamford, S. P., Aragón-Salamanca, A., Milvang-Jensen, B., Simard, L., 2004, submitted to MNRAS
Barbaro, G., Poggianti, B. M., 1997, A&A, 490, 504
Barger A. J., Aragón-Salamanca, A., Ellis, R. S., Couch, W. J., Smail, I., Sharples, R. M., 1996, MNRAS, 279, 1
Bartholomew, L. J., Rose, J. A., Gaba, A. E., Caldwell, N., 2001, AJ, 122, 2913
Bekki, K., 1998, ApJ, 502, L133
Bekki, K., 1999, ApJ, 510, L15
Bekki, K., & Shioya, Y., 1998, ApJ, 497, 108
Bekki, K., & Shioya, Y., 1999, ApJ, 513, 108
Bekki, K., Shioya, Y., Couch, W. J., 2001a, ApJ, 547, L17
Bekki, K., Couch, W. J., Shioya, Y., 2001b, PASJ, 53, 395
Bekki, K., Couch, W. J., Shioya, Y., 2002, ApJ, 577, 651
Bekki, K., Couch, W. J., 2003, ApJ, 596, L13
Bekki, K., Harris, W. E., Harris, G. L. H., 2003, MNRAS, 338, 587
Bekki, K., Beasley, M. A., Forbes, D. A., Couch, W. J., 2004, ApJ, 602, 730
Belloni, P., Bruzual, A. G., Thimm, G. J., Roser, H.-J., 1995, A&A, 297, 61
Bender, R. 1996, in New light on galaxy evolution, ed. R. Bender, R. Davies, IAU symp. 171, p181
Binney, J., & Tremaine, S., 1987 in Galactic Dynamics, Princeton; Princeton Univ. Press.
Blake, C., et al. 2004, MNRAS in press (astro-ph/0408536)
Butcher, H., Oemler, A., ApJ, 226, 559
Caldwell, N., Rose, J. A., Dendy, K., 1999, AJ, 117, 140
Charlot, S., Ferrari, F., Mathews, G. J., Silk, J., 1993, ApJ, 419, L57
Couch, W. J., Sharples, R. M., 1987, MNRAS, 229, 423
Couch, W. J., Barger, A. J., Smail, I., Ellis, R. S., Sharples, R. M., 1998, ApJ, 430, 121
Davies, R. L., et al. 2001, ApJ, 548, L33
Dressler, A., Gunn, J. E., 1983, ApJ, 270, 7
Dressler, A., Smail, I., Poggianti, B. M., Butcher, H., Couch, W. J., Ellis, R. S., Oemler, A., Jr., 1999, ApJS, 122, 51
Fioc, M., & Rocca-Volmerange, B., 1997, A&A, 326, 950
Fisher, D., Fabricant, D., Franx, M., van Dokkum, P., 1998, ApJ, 498, 195
Franx, M., 1993, ApJ, 407, L5
Friel, E. D. 1995, ARAA, 33, 381
Galaz, G., 2000, AJ, 119, 2118

Geha, M., Guhathakurta, P., van der Marel, R. P., 2002, AJ, 124, 3073
Goto, T., et al. 2003, PASJ, 55, 771
Hausman, M. A., Roberts, W. W., Jr., 1984, ApJ, 282, 106
Hernquist, L., 1990, ApJ, 356, 359
Hernquist, L., Barnes, J. E., 1991, Nature, 354, 210
Kennicutt, R. C. 1998, ARA&A, 36, 189
Kumai, Y., Basu, B., Fujimoto, M., 1993, ApJ, 404, 144
Larson, R. B., 1981, MNRAS, 194, 809
Larson, R. B., 1998, MNRAS, 301, 569
Mihos, J. C., Hernquist, L., 1996, ApJ, 464, 641
Miller, N. A., Owen, F. N., 2001, ApJ, 554, L25
Milvang-Jensen, B., Aragón-Salamanca, A., Hau, G. K. T., Jørgensen, I., Hjorth, J., 2003, MNRAS, 339, L1
Noguchi, M., Ishibashi, S., 1986, MNRAS, 219, 305
Navarro, J. F., Frenk, C. S., White, S. D. M., 1996, ApJ, 462, 563
Norton, S. A., Gebhardt, K., Zabludoff, A. I., Zaritsky, D., 2001, ApJ, 557, 150
Poggianti, B. M., Barbaro, G., 1996, A&A, 314, 379
Poggianti, B. M., Wu, H., 2000, ApJ, 529, 157
Poggianti, B. M., Smail, I., Dressler, A., Couch, W. J., Barger, J., Butcher, H., Ellis, E. S., Oemler, A., Jr., 1999, ApJ, 518, 576
Quintero, A., et al. 2004, ApJ, 602, 190
Rose, J. A., Gaba, A. E., Caldwell, N., Chaboyer, B. 2001, AJ, 121, 793
Schmidt, M., 1959, ApJ, 344, 685
Shioya, Y., Bekki, K., 2000, ApJ, 539, L29
Shioya, Y., & Bekki, K., Couch, W. J., 2001, ApJ, 558, 42
Shioya, Y., & Bekki, K., Couch, W. J., 2004, ApJ, 601, 654
Shioya, Y., & Bekki, K., 2005, in preparation
Smail, I., Morrison, G., Gray, M. E., Owen, F. N., Ivison, R. J., Kneib, J.-P., Ellis, R. S., 1999, ApJ, 525, 609
Sugimoto, D., Chikada, Y., Makino, J., Ito, T., Ebisuzaki, T., Umemura, M., 1990, Nature, 345, 33
Tran, K. H., Franx, M., Illingworth, G., Kelson, D. D., van Dokkum, P. 2003, ApJ, 599, 865
Tran, K. H., Franx, M., Illingworth, G., van Dokkum, P., Kelson, D. D., Magee, D., 2004, in preprint (astro-ph/0403484)
Wielen, R., 1977, A&A, 60, 263
Wirth, G. D., Koo, D. C., Kron, R. G., 1994, ApJ, 435, L105
Yang, Y., Zabludoff, A. I., Zaritsky, Dennis; Lauer, T. R., Mihos, J. C., 2004, ApJ, 607, 258
Vazdekis, A., Casuso, E., Peletier, R. F., Beckman, J. E., 1996, ApJS, 106, 307
Zabludoff, A. I., Zaritsky, D., Lin, H., Tucker, D., Hashimoto, Y., Shectman, S. A., Oemler, A., Kirshner, R. P., 1996, ApJ, 466, 104